

# Photochemical Dissipative Structuring, Proliferation and Evolution at the Origin of Life

Karo Michaelian

July 2, 2020

Department of Nuclear Physics and Application of Radiation, Instituto de Física, Universidad Nacional Autónoma de México, Circuito Interior de la Investigación Científica, Ciudad Universitaria, México D.F., Mexico, C.P. 04510.

`karo@fisica.unam.mx`

## Abstract

I describe the non-equilibrium thermodynamics and the photochemical mechanisms which may have been involved in the abiotic synthesis, proliferation, and complexation of the fundamental molecules of life from simpler and more common precursor molecules such as HCN, H<sub>2</sub>O and CO<sub>2</sub> under the long wavelength UVC and UVB solar photon flux prevailing at Earth's surface during the Archean. The fundamental molecules absorb strongly in this UV region and exhibit strong non-adiabatic coupling between their excited and ground states which endows them with efficient photon dissipative capacity (broad wavelength absorption and rapid radiationless deexcitation) indicative of their dissipative structuring at the origin of life. Proliferation of the molecule occurs if the photochemical dissipative structuring becomes autocatalytic. Evolution occurs when a concentration fluctuation near a bifurcation becomes amplified, resulting from the non-linearity due to the autocatalicity, leading the system to a new stationary state with a different molecular concentration profile of usually greater photon dissipative efficacy. This direction of evolution is predicted by the *universal evolution criterion* of classical irreversible thermodynamic theory established by Onsager, Glansdorff, and Prigogine. The example of the UV photochemical dissipative structuring, proliferation, and evolution of the nucleobase adenine is given. The kinetic equations are resolved under different environmental conditions providing the first non-equilibrium thermodynamic analysis of the photochemical structuring of adenine.

**keywords:** origin of life; dissipative structuring; prebiotic chemistry; adenine

## 1 Introduction

There are two coexisting classes of structures in nature; *equilibrium structures* and *non-equilibrium structures*. Equilibrium structures arise naturally and their synthesis from arbitrary distributions of material can be described through the minimization of a thermodynamic potential, for example, a crystal structure arising from the minimization of the Gibbs potential at constant temperature and pressure. The second class is of non-equilibrium structures known as *dissipative structures* which also arise naturally through the optimization of the dissipation of an externally imposed generalized thermodynamic potential (1), for example the “spontaneous” emergence of convection cells arising to increase the thermal dissipation at a critical value of an imposed temperature gradient.

Life, although incorporating equilibrium structures, is fundamentally a non-equilibrium process and therefore its existence is dependent on the dissipation of one or more thermodynamic potentials in its environment. Boltzmann recognized this almost 125 years ago (2) and suggested that life dissipates the solar photon potential (3). Present day life has evolved to dissipate other thermodynamic potentials accessible on Earth's surface, for example, chemical potentials available in organic or inorganic molecules or available in gradients at hydrothermal vents. However, UV light would have provided an approximately three orders of magnitude greater, and continuous, source of free energy than volcanic activity and electric discharge combined (4; 5; 6), irrespective of a more radioactive Archean Earth. This UV wavelength solar photon flux was continually available at Earth's surface for over 1000 million years during the Archean and thus could have provided the dissipative potential for not only for molecular synthesis, but also for molecular proliferation and the evolution towards a biosphere of ever greater global photon dissipation. Furthermore, the free energy available to a precursor molecule for covalent bond transformation is orders of magnitude greater

for photochemical reactions than for thermal reactions (section 3). There is, therefore, much greater rationale in the conjecture that the solar photon potential, rather than some chemical potential, was responsible for the original dissipative structuring, proliferation, and evolution of the fundamental molecules of life (those common to all three domains).

We have identified the long wavelength part of the UVC ( $\sim 210\text{-}285\text{ nm}$ ), plus the short wavelength part of the UVB ( $\sim 310\text{-}360\text{ nm}$ ), solar photon spectrum as the thermodynamic potential which probably drove the dissipative structuring, proliferation, and evolution relevant to the origin of life (7; 8). This light prevailed at Earth's surface from the Hadean, before the probable origin of life near the beginning of the Archean ( $\sim 3.9\text{ Ga}$ ), and for at least 1000 million years (9; 10; 11) until the formation of an ozone layer when natural oxygen sinks (for example, free hydrogen and  $\text{Fe}^{+2}$ ) became overwhelmed by organisms performing oxygenic photosynthesis.

A strong argument in favor of the conjecture that the fundamental molecules of life resulted from dissipative structuring under this wavelength region, corresponding to Archean atmospheric transparency (figure 1), is that longer wavelengths do not contain sufficient free energy to directly break double covalent bonds of carbon based molecules, while shorter wavelengths have enough energy to destroy these molecules through successive ionization and fragmentation.

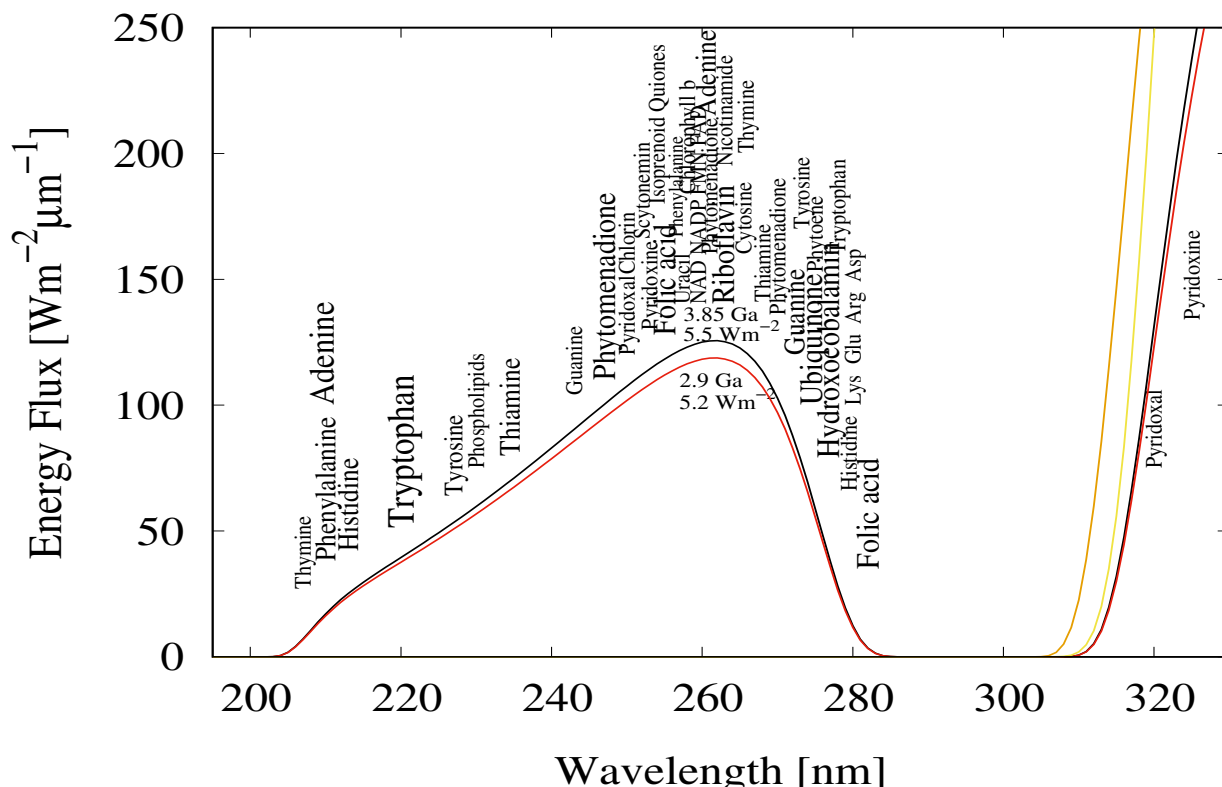


Figure 1: The spectrum of light available in the UVC and UVB regions at Earth's surface during the Archean. The names of the fundamental molecules of life (nucleic acids, amino acids, fatty acids, co-enzymes and co-factors) are plotted at their wavelengths of maximal absorption (the font size of the letter roughly corresponds to the relative size of their molar extinction coefficient) and coincide with this predicted atmospheric window which existed from before the origin of life at approximately 3.85 Ga and until at least 2.9 Ga (curves black and red respectively).  $\text{CO}_2$  and probably some  $\text{H}_2\text{S}$  were responsible for absorption at wavelengths shorter than  $\sim 205\text{ nm}$  and atmospheric aldehydes (common photochemical products of  $\text{CO}_2$  and water) absorbed between approximately 285 and 310 nm (10). Around 2.2 Ga (yellow curve), UVC light at Earth's surface had been extinguished by oxygen and ozone resulting from organisms performing oxygenic photosynthesis. The green curve corresponds to the present surface spectrum. Energy fluxes are for the sun at the zenith. Adapted from Michaelian and Simeonov (12).

Numerous empirical evidences also support the conjecture of the dissipative structuring of the fundamental molecules of life under these wavelengths. First, the maximum in the strong absorption spectrum of many of these molecules coincides with the predicted window in the Archean atmosphere (Fig. 1). Secondly, many of the funda-

mental molecules of life are endowed with *peaked conical intersections* (section 3.2) giving them a broad absorption band and high quantum yield for rapid (picosecond) dissipation of the photon-induced electronic excitation energy into vibrational energy of molecular atomic coordinates, and finally into the surrounding water solvent. Perhaps the most convincing evidence of all, however, is that many photochemical routes to the synthesis of nucleic acids, amino acids, fatty acids and sugars from simple, presumably common, precursor molecules have been identified at these wavelengths and the rate of photon dissipation within the Archean window generally increases after each incremental step on route to synthesis (13; 14), a behavior strongly suggestive of dissipative structuring (section 2).

In contradistinction to the generally held view that UV wavelengths were detrimental to early life and thereby induced extreme selection pressure for mechanisms or behavioral traits that protected life from, or made life tolerable under, these photons (10; 15; 16; 17), here I argue that these wavelengths were not only fundamental to the photochemical synthesis of life's first molecules (as suggested with increasing sophistication by Oparin (18), Haldane (19), Urey (20), Sagan (21) and Mulikidjanian (17) and supported experimentally by Baly (22), Miller (23), Oro and Kimball (24), Ponnampetuma et al. (25; 26; 27), Ferris and Orgel (28), and Sagan and Khare (29) as well as others) but that this UV light was fundamental to the origin and early existence of the entire thermodynamic dissipative process known as "life" comprising of synthesis, proliferation, and evolution (section 2) leading to biosphere complexation with concomitant increases in photon dissipation over time. Rather than seeking refuge or procuring protection from this UV light, it is argued here that molecular transformations providing innovations which allowed early life to maximize UV exposure; e.g. buoyancy at the ocean surface, larger molecular antennas for capturing this light, increases in the width of the wavelength absorption band, and peaked conical intersections providing extraordinarily low antenna dead-times, would all have been thermodynamically selected for. Indeed, there exists empirical evidence suggesting selection for traits optimizing UV exposure for particular amino acids complexed with their RNA or DNA cognate codons, particularly for those amino acids displaying the strongest stereochemical affinity to their codons or anticodons (30). This has led us to suggest that UVC photon dissipation was the basis of the initial specificity in the amino acid - codon association during an early stereochemical era (31).

Life may thus be identified with a particular form of dissipative structuring; *microscopic* dissipative structuring of carbon based molecules under UVC light in which the synthesized products, the fundamental molecules, were initially UVC pigments which demonstrated stability for long periods due to their peaked conical intersections which dramatically reduces the quantum efficiency for deexcitation through further photochemical reaction pathways. Unlike macroscopic dissipative structures such as hurricanes or convection cells, at normal temperatures these microscopic dissipative structures remain intact even after the removal of the imposed light potential driving their synthesis due to strong covalent bonding between atoms.

I will show in section 4 that if intermediate product molecules on route to the dissipative synthesis of the fundamental molecules are catalysts for the photochemical reactions, then this would lead to their proliferation, as well as to that of their final product molecules. Efficacy in dissipation will be shown to be selected for by an established non-equilibrium thermodynamic criterion (section 2) and this, along with proliferation, provides a mechanism for evolution which may be termed *dissipative selection*, or more generally, *thermodynamic selection*. Dissipative structuring, dissipative proliferation, and dissipative selection, are the necessary and sufficient elements for a non-equilibrium thermodynamic framework from within which the origin and evolution of life can be explained in physical and chemical terms (7; 8; 3).

The perspective taken here, therefore, is that the origin of life was not a scenario of organic material organization driven by natural selection leading to "better adapted" organisms, or to greater chemically stability (e.g. UV resistant organisms), but rather a scenario of the dissipative structuring of material under the imposed UV solar photon potential leading to an organization of material in space and time (biosynthetic pathways) providing more efficient routes to the dissipation of the externally imposed photon potential. The dissipative synthesis of an ever larger array of photochemical catalysts and cofactors, would mean that ever more complex biosynthetic pathways would emerge through *thermodynamic selection* to promote the synthesis of novel pigments for dissipating not only the fundamental UVC and UVB regions, but eventually the entire short wavelength region of the solar photon spectrum (12; 32), eventually reaching the red-edge ( $\sim 700$  nm) which is the approximate limit of biological photon dissipation on Earth today.

There exists many proposals, supported by a large body of empirical data, for the exogenous delivery (comets, meteorites, and space dust) or endogenous synthesis (atmospheric, ocean surface, warm ponds, hydrothermal vents) of the fundamental molecules of life. Free energy sources proposed for synthesis on Earth include; meteoric shock impact, electric discharge, high temperature, temperature gradient, pH gradient, particle radiations, gamma rays, UV light, organocatalysis, micro forces, etc. However, a robust explanation of life requires a clear understanding as to not only how biologically important molecules spontaneously emerged, but how they proliferated and evolved into ever more complex macroscopic structures building a global dissipative process known as the *biosphere*.

“Information first” theories for the origin of life inevitably decay into equilibrium since little or no attention is paid to the dissipation of an externally imposed generalized thermodynamic potential. “Metabolism first” theories recognize the need for a free energy source for synthesis and homeostasis but fail to recognize the association of increasing dissipation with proliferation and evolution. The thermodynamic dissipation theory for the origin of life (8; 3), employed as the framework here, assigns an explicit thermodynamic function to life; *life is the dissipative structuring, proliferation, and evolution of molecular pigments and their complexes from common precursor carbon based molecules under the imposed short wavelength solar photon potential for performing the explicit thermodynamic function of dissipating this light into long wavelength infrared light (heat)*. The external photon potential supplied continuously by the environment, and its dissipation into heat by the spontaneously-assembled dissipative structures, are both integral parts of our definition of life.

## 2 Thermodynamic Foundations of Microscopic Dissipative Structuring, Proliferation, and Selection

Irreversible processes can be identified by the distribution (flow) of conserved quantities (e.g. energy, momentum, angular momentum, charge, etc.) over an increasing number of microscopic degrees of freedom, often involving, at the macroscopic scale, spatial coordinate degrees of freedom. Corresponding to a given flow there exists a conjugate generalized thermodynamic force. For example, to the macroscopic flows of heat, matter, and charge, over coordinate space, there corresponds the conjugate forces of minus the gradient of the inverse of temperature, minus the gradient of mass density (concentration gradient), and minus the gradient of the electric charge density (the electrostatic potential) respectively. Flows of the conserved quantities can occur not only over macroscopic coordinate degrees of freedom, but also over molecular degrees of freedom, such as over electronic or vibrational coordinates, spin coordinates, and reaction coordinates (ionizations, deprotonations, charge transfer, disassociations, isomerizations, tautomerizations, rotations around covalent bonds, sigmatropic shifts, etc.), obeying statistical quantum mechanical rules. The corresponding conjugate forces to these flows of the conserved quantities involved in the molecular processes of life are electromagnetic in nature, for example, the chemical and photochemical potentials. Since, for covalent, strongly bonded organic material, access to these molecular degrees of freedom usually requires the deposition of a large amount of the conserved quantity (e.g. energy) locally (e.g. on a particular region of a molecule), such flow, and any resulting dissipative structuring occurring at the origin of life (before the evolution of complex biosynthetic pathways) was necessarily associated with ultraviolet photon absorption.

The existence of any macroscopic flow, or equivalently any unbalanced generalized thermodynamic force, necessarily implies that the system is not in thermodynamic equilibrium. Under the assumption of *local thermodynamic equilibrium* (e.g., local Maxwell-Boltzmann distribution of particle velocities or excited vibrational states), Onsager, Prigogine, Glansdorff, Nicolis, and others developed the mathematical framework to treat out-of-equilibrium phenomena known as “Classical Irreversible Thermodynamics” (CIT) (1). In this framework, the total internal (to the system) entropy production  $P$  per unit volume,  $\sigma \equiv P/V = (d_i S/dt)/V$ , of all irreversible processes occurring within the volume due to  $n$  generalized thermodynamic forces  $k = 1, n$  is simply the sum of all forces  $X_k = A_k/T$  (where  $A_k$  are the affinities and  $T$  is the temperature) multiplied by their conjugate flows  $J_k$ . This sum, by the local formulation of the second law of thermodynamics (1), in any macroscopic volume, is positive definite for irreversible processes and equal to zero for reversible processes (those occurring in thermodynamic equilibrium),

$$\sigma \equiv \frac{P}{V} = \frac{d_i S/dt}{V} = \sum_{k=1,n} X_k J_k = \sum_{k=1,n} \frac{A_k}{T} J_k \geq 0. \quad (1)$$

The validity of the assumption of local equilibrium for the case studied here, of molecular photochemical dissipative structuring of the fundamental molecules, requires that the absorbed energy of the incident photon becomes distributed with Boltzmann statistics over the nuclear vibrational degrees of freedom implicated in molecular transformations (hot excited or hot ground state reactions). Note that the Franck-Condon principle implies that the electronically excited molecule will most likely be in a vibrationally excited state. Organic materials in the liquid or condensed phase are generally “soft materials” in the sense that their vibrational degrees of freedom in the electronic excited state couple significantly to their vibrational degrees of freedom in the electronic ground state (unlike in the case of inorganic material). This nonadiabatic coupling is mediated by conical intersections which allow for ultra-fast equilibration of the photon energy over the vibrational degrees of freedom of the electronic ground state (see 3.2), often on sub-picosecond time scales, leaving small molecules for a short time (depending on the nature of their surroundings) with an effective vibrational temperature of 2000-4000 K. This time for vibrational equilibration is generally less than the time required for a typical chemical transformation and therefore the irreversible

process of molecular dissipative photochemical structuring can be justifiably treated under the CIT framework in the non-linear regime. (Here, the “non-linear regime” refers to the fact that chemical - and photochemical - reactions are inherently non-linear in that the flow (the rate of the reaction) is not linearly proportional to the force (the affinity over the temperature) except near equilibrium where affinities are small.) Indeed, Prigogine has shown that irrespective of the imposed affinities, chemical reactions in the electronic ground state can be treated successfully under CIT theory as long as the reactants retain a Maxwell-Boltzmann distribution of their velocities, which is the case for all but very exothermic (explosive) reactions (1).

The time change of the total entropy production  $P$  for any out-of-equilibrium system can be split into two parts, one depending on the time change of the forces  $X$ , and the other on the time change of the flows  $J$ ,

$$\frac{dP}{dt} = \frac{d_X P}{dt} + \frac{d_J P}{dt}, \quad (2)$$

where, for a continuous system within a volume  $V$ ,

$$\frac{d_X P}{dt} = \int \sum_{k=1,n} J_k \frac{dX_k}{dt} dV, \quad \frac{d_J P}{dt} = \int \sum_{k=1,n} X_k \frac{dJ_k}{dt} dV, \quad (3)$$

For the case of constant external constraints over the system, for example when affinities  $\mathcal{A} = \{A_k; k = 1, c\}$  are externally imposed and held constant, CIT theory indicates that the system will evolve towards a stationary state in which its thermodynamic state variables (for example, the internal energy  $E$ , entropy  $S$ , and entropy production  $P = d_i S/dt$ ) become time invariant. For flows linearly related to their forces, it is easy to show that there is only one stationary state and that the entropy production in this stationary state takes on its minimal value with respect to variation of the free affinities  $\mathbf{A} = \{A_k; k = c + 1, n\}$  in the system (1). This principle of minimum dissipation for linear systems was first proposed by Lord Rayleigh in 1873 (33).

However, if the flows are non-linearly related to the forces (e.g. for chemical reactions the rates of the reaction (flows) are proportional to the difference in the reactant and product concentrations, while the affinities (forces) are proportional to the logarithm of these concentration ratios), then, depending on the number of degrees of freedom and how non-linear the system is, at a certain value of a variable of the system (e.g. overall affinity), labeled a *critical point*, the system becomes unstable and new, possibly many, different stationary states become available, each with a possibly different value of internal entropy production  $P = d_i S/dt$ . In this case, stationary states are only locally stable in some variables of the system, or even unstable in all variables. The non-linear dynamics is such that different stationary states, corresponding to different sets of flows  $\mathbf{J}_\alpha, \mathbf{J}_\beta$ , etc. conjugate to their sets of free affinities  $\mathbf{A}_\alpha, \mathbf{A}_\beta$ , etc. become available through current fluctuations  $\delta\mathbf{J}_\alpha, \delta\mathbf{J}_\beta$ , etc., at the critical instability point (or bifurcation point) along a particular variable of the system, because, unlike in the equilibrium or in the linear non-equilibrium regimes, in the non-linear non-equilibrium regime these microscopic fluctuations  $\delta\mathbf{J}_\alpha$  on their original flows  $\mathbf{J}_\alpha$  can be amplified through feedback (e.g. autocatalysis) into new macroscopic flows  $\mathbf{J}_\beta$  (1).

Since for such a non-linear system, under an externally imposed thermodynamic force, multiple stationary states are available, an interesting question arises concerning the stability of the system and how the system may evolve over time between different stationary states. Because the system harbors critical points at which microscopic fluctuations can be amplified into macroscopic flows leading the system to a new stationary state, it cannot be expected that there exists a potential for the system whose optimization could predict its evolution. What could be hoped for, however, is a statistical rule governing relative probabilities for the different evolutionary trajectories over the stationary states.

Prigogine and co-workers have shown that, although in general no optimizable total differential (thermodynamic potential) exists for these non-linear systems, there does, however, exist a non-total differential, the time variation of the entropy production with respect to the time variation of the free forces  $d_X P/dt$  (see equation 2), which always has a definite sign,

$$\frac{d_X P}{dt} \leq 0. \quad (4)$$

This is the most general result so far obtained from CIT theory, valid in the whole domain of its applicability, independent of the nature of the relation between the flows and forces. It is known as the *universal evolution criterion*, or sometimes called the *Glansdoff-Prigogine criterion*. This criterion indicates that the free forces always arrange themselves within a system such that this arrangement contributes to a decrease in the entropy production. However, in general, there is no such restriction on the total entropy production of the system because this also includes a component due to the corresponding rearrangement of the flows (see Eqn. (2)) which has no definite sign. The total entropy production may either increase or decrease during evolution in the nonlinear regime, depending on the relative signs and sizes of the two terms in equation (2). In the regime of linear phenomenological

relations (a linear relation between the flows and forces), it is easy to show (1) that  $d_J P/dt = d_X P/dt$  and thus the universal evolutionary criterion, Eq. (4), correctly predicts the theorem of minimum entropy production alluded to above,  $dP/dt \leq 0$ . The stability in the Lyapunov sense of the unique stationary state in this linear regime is then guaranteed by the fact that the entropy production is a Lyapunov function (i.e.  $P > 0$  and  $dP/dt \leq 0$ ).

Given that, in the nonlinear regime, bifurcations can be reached leading to multiple stationary states (which for the case studied here of the photochemical dissipative structuring of the fundamental molecules of life corresponds to different concentration profiles of the distinct molecular configurations involved in the synthesis, each profile having a potentially different rate of dissipation of the applied photon potential), it is pertinent to inquire if there indeed exists certain statistical probabilities (as alluded to above) regarding the direction of evolution of the system in terms of the total entropy production. In this non-linear regime with multiple stationary states, the local stability of each stationary state has to be evaluated individually and the probability of evolution constrained by equation (4) from one state to another has to be evaluated through a local stability analysis which ultimately concerns the size of the fluctuations, the size of the barriers in  $d_X P$ , and the size of the catchment basins of neighboring stationary states in a generalized phase space. For the dissipative synthesis of the fundamental molecules of life, we will see that the size of these catchment basins is related to the number of conical intersections associated with a particular molecular photochemical transformation and their “peakedness” (section 3), and the accessibility of these is related to the size of the free energy barriers on route to the conical intersections from the excited state nuclear coordinates initially in the Franck-Condon region (having the unperturbed ground state nuclear coordinate configuration).

Even though  $d_X P$  is not a total differential, it can still be used to determine the nature and local stability of each stationary state, not only in the linear regime as shown above, but also in the non-linear regime. To illustrate the dissipative structuring of a fundamental molecule under UVC light and the utility of the universal evolution criterion ( $d_X P \leq 0$ ) in determining probabilities for paths of evolution among multiple stationary states (distinct concentration profiles), in section 4 I present an example of the non-equilibrium thermodynamics and photochemical kinetics of the synthesis of adenine from 5 molecules of hydrogen cyanide (HCN) (see figure 3) in water under the impressed UVC photon spectrum of the Archean given in figure 1. Such a photochemical route to adenine was discovered experimentally by Ferris and Orgel in 1966 (28) and we have suggested that this may be an example of dissipative structuring under a UVC+UVB photon potential (13). It will be seen how the evolution of the concentration profile of the intermediate molecules over different stationary states under the *universal evolution criterion* leads to an increase in adenine concentration and a concomitant increase in global photon dissipation. First, however, it is pertinent to delineate the photochemistry available to carbon based organic molecules undergoing dissipative structuring.

## 3 Photochemistry

### 3.1 Quantum Selection Rules

Absorption by an organic molecule of a visible or UV photon of the required energy  $E = h\nu$  leads to an electronic spin singlet or triplet excited state. The width of the allowed transition  $\Delta E$  is determined by the natural line width dependent on the natural lifetime  $\Delta t$  of the excited state, as given by the Heisenberg uncertainty relation  $\Delta E \Delta t \geq \hbar$ . In condensed material or at high pressure, further broadening occurs due to deexcitation through collisions with neighboring molecules, reducing further the lifetime. There is also a broadening due to the Doppler effect which increases with temperature. Most importantly, however, for the organic molecules considered here, there is a broadening due to the coupling of electronic degrees to the vibrational degrees of freedom of the molecule (vibronic or non-adiabatic coupling).

Excitation to the triplet state is a spin forbidden transition but can occur due to spin-orbit coupling or interaction with a paramagnetic solvent molecule, for example oxygen in its spin-triplet ground state. Under laboratory conditions and for organic molecules, however, the singlet state is favored over the triplet state by  $\sim 1000 : 1$ . Moreover, since electronic excitations are affected by the electronic dipole transition which is first order in the coordinates  $x$  (i.e. the dipole moment is an odd function  $f(x) \neq f(-x)$ ), and since an additional quantum selection rule is that transitions must be symmetric, the symmetries of the wavefunctions of the molecule in the initial and final state must be different (e.g. even  $\rightarrow$  odd) giving rise to the electronic angular momentum selection rule  $\Delta l = \pm 1$ . For example, a  $1S \rightarrow 2S$  transition is forbidden while a  $1S \rightarrow 2P$  transition is allowed.

## 3.2 Conical Intersections

The Born-Oppenheimer approximation in molecular structure calculations assumes independence of the electronic and nuclear motions. However, such an approximation is obviously not valid for chemical reactions where nuclear reconfiguration is coupled to electronic redistribution and particularly not valid for photochemical reactions where the potential energy surface of an electronic excited state is reached.

Conical intersections are multi-dimensional seams in nuclear coordinate space where the adiabatic potential energy surface of the electronic excited state becomes degenerate with the potential energy surface of the electronic ground state of the same spin multiplicity, resulting from a normally barrier-less out of plane distortion of the nuclear coordinates (e.g. bond length stretching or rotation about a bond). A common distortion of the nuclear coordinates for the excited state of the nucleobases is ring puckering as shown for adenine in figure 3.2. This multi-dimensional seam, defining the energy degeneracy, allows for rapid (sub-picosecond) radiationless dexcitation of the photon-induced electronic excited state, distributing the electronic energy over nuclear vibrational modes of the molecule and solvent, thereby producing entropy and leaving the molecule in the ground state ready for another photon absorption event.

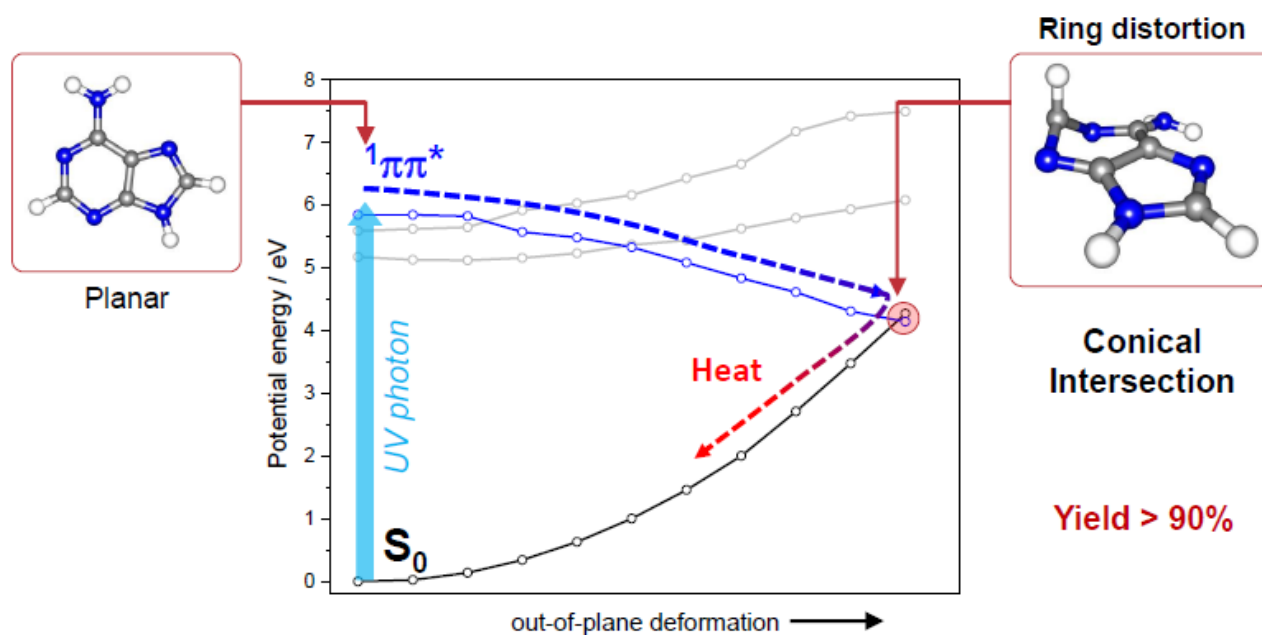


Figure 2: Conical Intersection for adenine showing the degeneracy of the electronic excited state with the electronic ground state after a UVC photon absorption event which induces a nuclear coordinate deformation known as *pyrimidilization*. Conical intersections provide rapid (sub-picosecond) dissipation of the original electronic excitation. Another common form of coordinate transformation associated with conical intersections are proton transfers within the molecule or with the solvent. Reproduced from Andrew Orr-Ewing (34) based on Kleinermanns et al. (35) and Barbatti et al. (36)

Besides providing a route for the energy dissipation in excited molecules, conical intersections also supply a route for charge flow and thus define the photoisomerization or photoreaction products that can be reached after an excitation event. Since conical intersections are located energetically down-hill from the Franck-Condon region, the direction and velocities of approach of the nuclear coordinates to a conical intersection are important in defining the outcome (37). The shape of the conical intersection seam determines the rate of dissipation and influences the final isomerization, tautomerization, or reaction product. For example, it is known that for the molecule retinal in rhodopsin the photoexcited molecule reaches the conical intersection extremely fast (75 femtoseconds) implying that the conical intersection must be peaked (inverted cone-like on the excited state potential energy surface) and, overwhelmingly, only one reaction product is reached, which for the case of retinal, as well as for the fundamental molecules of life, is the original ground state configuration (38). A more extended seam with different minima can lead to different reaction products (39) such as those intermediates on route to the photochemical synthesis of the

fundamental molecules which will be described below. The final product in the photochemical synthesis of the fundamental molecules of life, however, always has a peaked conical intersection and therefore becomes the *final* and *stable* photoproduct of dissipative structuring in the relevant region of the solar spectrum.

It has been a recurrent theme in the literature that the rapid (sub picosecond) deexcitation of the excited nucleobases due to their conical intersection had evolutionary utility in providing stability under the high flux of UV photons that penetrated the Archean atmosphere (10; 17) since the conical intersection reduced the lifetime of the excited state to the point where further chemical reactions were no longer very probable. However, photochemical reactions under UVC light still do occur for the fundamental molecules of life, particularly after excitation to the long lived triplet state, for example in the formation of cyclobutane pyrimidine dimers in RNA and DNA. An apparently more optimal and simpler solution for avoiding radiation damage with its concomitant degradation in biological function, therefore, would have been the synthesis of molecules transparent or reflective to this UV light. From the thermodynamic perspective of dissipation presented here, however, a large antenna for maximum UVC photon absorption and a conical intersection for rapid dissipation into heat are, in fact, the design goals of dissipative structuring.

### 3.3 Excited State Reaction Mechanisms

The photochemistry of molecules in electronic excited states is much richer than the thermal chemistry of their ground state, because; 1) the available energy conferred to the molecule by the absorbed photon allows very endothermic reactions to occur, 2) anti-bonding orbitals are occupied in the excited state, allowing reactions to occur that, because of electronic considerations, are prohibited in the ground state, 3) triplet states can be reached from the electronic excited state, allowing for the production of intermediates that cannot be accessed in thermal reactions, 4) molecules are often converted into radicals in the excited state, making them much more reactive. A molecule in its excited state can be a much stronger oxidizer or reductor having a  $pK_a$  value substantially different from that of the molecule in its ground state. For example, if the  $pK_a$  value becomes more acidic, proton transfer to an acceptor solvent water molecule may occur. Singlet excited states have a particularly rich chemistry, while triplet states have a more restricted chemistry but provide more time for vibrational equilibration. This richness in chemistry is, in itself, yet another strong argument in favor of the complex molecules of life arising out of photochemical reactions at the surface of the ocean rather than, for example, thermal reactions occurring at the bottom of the ocean.

Photochemical processes that arise after photon-induced excitation can be classified into dissasociations, rearrangement, additions and substitutions. Each process constitutes a particular mechanism for molecular transformation which could have been employed in the photochemical dissipative structuring of the fundamental molecules at the origin of life under the UVC photon potential. Indeed, these mechanisms still occur today in many important photochemical processes of life, albeit in the visible and through much more complex biosynthetic pathways.

The photochemical transformations listed above generally have a strong dependence on wavelength due to the particular absorption characteristics of the inherent chromophores of the precursor molecules. However, it is not only the absorption coefficient of the chromophore which is important since within a given wavelength region there may be two or more such molecular transformational processes in competition, and therefore the particular conformation of the electronic ground state before excitation may be relevant. This conformation could depend on the temperature, viscosity, polarity, ionic strength and pH of the solvent, all of which are determinant in the yields of the final photoproducts.

Some of the molecular transformations mentioned above do not belong exclusively to the domain of photochemical reactions but can also occur through thermal reactions at high temperature, albeit with lower yield and less variety of product. Therefore, some of the fundamental molecules of life could have been produced through thermal mechanisms without recourse to the incident light, for example at ocean floor hydrothermal vents. However, as emphasized in the introduction, the mere synthesis of the fundamental molecules should not be misconstrued as being equivalent to bootstrapping the irreversible dissipative process known as life. The continuous dissipation of an external thermodynamic potential is a necessary condition for the structuring, proliferation, and evolution of life, as it is for any sustained irreversible process.

## 4 Example: The Dissipative Structuring of Adenine

### 4.1 Overview of the Model

HCN is a common molecule found throughout the cosmos and its production during the Hadean and Archean on Earth was probably a result of the solar Lyman alpha line (121.6 nm) photo-lysing  $N_2$  in the upper atmosphere which then attacks CH or  $CH_2$  to form HCN (40), or the UV (145 nm) photolysis of  $CH_4$  leading to a  $CH^*$  radical which attacks  $N_2$  (40). HCN and its hydrolysis product formamide are now recognized as probable precursors of many of the fundamental molecules of life, including nucleic acids, amino acids, fatty acids (41), and even simple sugars (42; 43). As early as 1875 E. Pflüger suggested that life may have followed from “cyanogen compounds” (44). The ubiquity of different chemical and photochemical routes from HCN to the fundamental molecules discovered over the last 60 years has led to the suggestion of an “HCN World” (45; 46) occurring before the postulated “RNA World” (47).

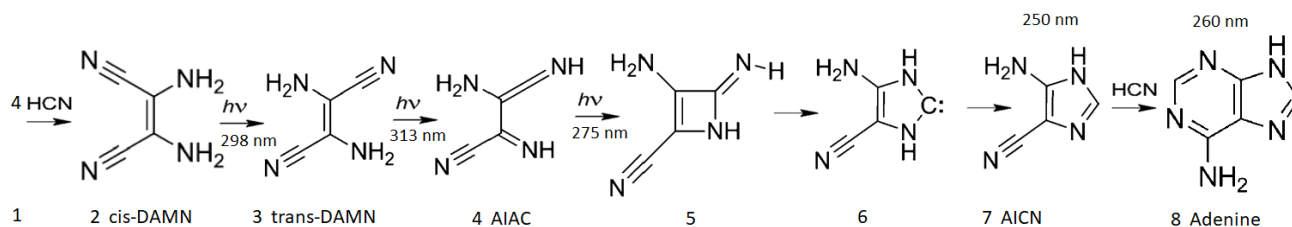


Figure 3: The photochemical synthesis of adenine from 5 molecules of hydrogen cyanide (HCN) in water, as discovered by Ferris and Orgel (1966) (28; 48). This is a dissipative structuring process that ends in adenine which has a large molar extinction coefficient and a peaked conical intersection at 260 nm promoting the dissipation of photons at the wavelength of maximum intensity of the Archean spectrum (figure 1). Four molecules of HCN are transformed into the smallest stable oligomer (tetramer) of HCN, known as cis-2,3-diaminomaleonitrile (cis-DAMN) (2), which, under a constant UV-C photon flux isomerizes into trans-DAMN (3) (diaminofumarionitrile, DAFN) which may be further converted on absorbing two more UV-C photons into an imidazole intermediate, 4-amino-1H-imidazole-5-carbonitrile (AICN) (7). Hot ground state thermal reactions with another HCN molecule or its hydrolysis product formamide (or ammonium formate) leads to the purine adenine (8). Adapted from Ferris and Orgel (1966)(28)

The synthesis of adenine from HCN has been studied by numerous groups since the first experimental observations of the chemical reaction at high temperatures by Oró in 1960 (49) and photochemically at moderate temperatures by Ferris and Orgel in 1966 (28; 50; 51; 52; 48). Adenine is a pentamer of HCN and the overall reaction from 5 HCN to adenine is exothermic ( $\Delta G = -53.7 \text{ kcal mol}^{-1}$  (52)) but presents a number of large kinetic barriers which can be overcome at high temperatures or at low temperatures if UV photons are absorbed. The reactions on route to adenine are in competition with hydrolysis and UV lysis, and these relative rates are dependent on concentrations, temperature, pH, metal ion- and product- catalysis, and the wavelength dependent intensity of the incident UV spectrum. The complexities involved in the photochemical reactions leading to adenine have been studied by Sanchez et al. (50; 51).

An apparent difficulty arose with respect to the synthesis of the purines from HCN in that, for dilute concentrations of HCN ( $< 0.01 \text{ M}$ ), hydrolysis of HCN occurs at a rate greater than its polymerization, e.g. its tetramerization (step 1 to 2, figure 3), the first step on route to adenine. Hydrolysis is proportional to the HCN concentration whereas tetramerization is proportional to the square of the concentration (50). Stribling and Miller (53) estimated that atmospheric production of HCN and subsequent loss to hydrolysis, would have led to ocean concentrations at neutral pH no greater than about  $1.0 \times 10^{-12} \text{ M}$  at  $100^\circ \text{C}$  and  $1.0 \times 10^{-4} \text{ M}$  at  $0^\circ \text{C}$  for an ocean of 3 Km average depth. This led Sanchez, Miller, Ferris, Orgel (54; 50) to conclude that eutectic concentration of HCN (through freezing) would have been the only viable route to synthesis of the purines, and this is the primary reason why subsequent analyses favored a cold scenario for the origin of life (55; 56; 57), notwithstanding the geochemical evidence to the contrary, and even though this severely reduces all reaction rates and inhibits diffusion.

However, it is now known that the top  $\sim 100 \mu\text{m}$  of the ocean surface (known as the microlayer) is a unique environment with the density of organic material being as large as  $10^4$  times that of bulk water below. This is due

to lowering of the free energy of fatty acids and other amphiphathic molecules at the air/water interface, as well as Eddy currents and air bubbles from raindrops bringing organic material to the surface (58; 59). Furthermore, it has been shown that even though HCN is very soluble in water (and even in non-polar solvents), it tends to concentrate at a water surface and is observed to align itself through a dipole-dipole interaction in such a manner so as to facilitate polymerization. Molecular dynamic simulations of HCN in water have shown that it can form patches of significantly higher density in both the lateral and vertical dimensions at the surface, due to this rather strong dipole-dipole interaction between molecules (60).

Our model, therefore, rather than relying on eutectic concentration to increase the solute HCN concentration to values sufficient for significant adenine production, assumes instead the existence at the surface of fatty acid vesicles of  $\sim 100 \mu\text{m}$  diameter which would allow the incident UVC light, as well as small molecules such as HCN, to enter relatively unimpeded by permeating its bi-layer wall (see figure 4), while trapping within the vesicle the photochemical reaction products due to their larger sizes and larger dipole moments (table 1). This would allow these molecules, as well as the heat of their UV photon dissipation, to accumulate within the vesicle. The existence of hydrocarbon chains which spontaneously form lipid vesicles at the ocean surface is a common assumption in origin of life scenarios and their probable existence during the Archean has been attributed to heat activated Fischer-Tropsch polymerization of smaller hydrocarbon chains such as ethylene at very high temperatures at deep ocean vents, or to dissipative structuring under UVC photons of  $\text{CO}_2$  saturated water at lower temperatures on the ocean surface (14). In order to maintain vesicle integrity at the hot surface temperatures considered here of  $\sim 80^\circ\text{C}$  these fatty acids would necessarily have been long ( $\sim 18$  C atoms) and cross linked through UVC light which improves stability at high temperatures and over a wider range of pH values (61; 14). There is, in fact, a predominance of 16 and 18 carbon atom fatty acids in the whole available Precambrian fossil record (62; 63).

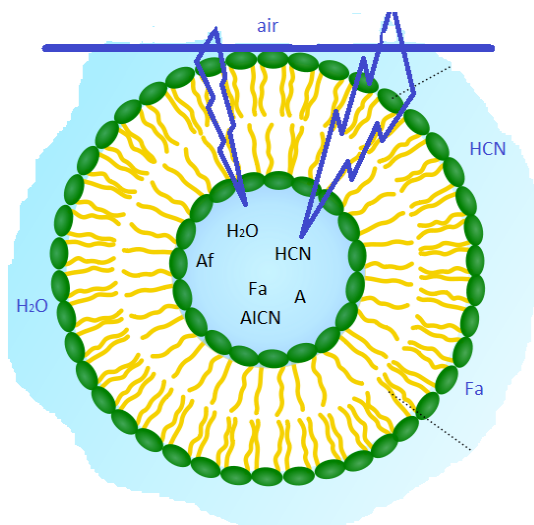


Figure 4: Fatty acid vesicle of  $\sim 100 \mu\text{m}$  diameter floating at the ocean surface microlayer, transparent to UVC light and permeable to  $\text{H}_2\text{O}$ , HCN and formimidic acid (Fa) but impermeable to the photochemical reaction products (e.g. ammonium formate (Af), AICN, adenine (A)).

In the following subsection I present a simplified out-of-equilibrium kinetic model for our  $5\text{HCN} \rightarrow$  adenine photochemical reaction system occurring within a fatty acid vesicle floating within the surface microlayer of a hot ( $\sim 80^\circ\text{C}$  (64; 65; 66)) Archean ocean. I assume that the system is under a diurnal 8 hr flux of radiation having the spectrum presented in figure 1, including a corresponding 8 hour period of darkness during which thermal reactions occur but not photochemical reactions. I assume the existence of patches of relatively high concentration (0.01 M) of HCN and formimidic acid (Fa), a photon-induced tautomer of its hydrolysis product formamide (F), into which our vesicle drifts periodically, and remains immersed within for short periods (120 seconds), say once every 3.5 Archean days.

The kinetic equations for the above model are resolved numerically, and the stationary state solutions obtained. For such a non-linear reaction-diffusion system it will be shown in section 5 that stationary state solutions exist with the highest concentration of adenine at the center of the vesicle, sufficient, in fact, to permit a subsequent UVC polymerization of the purines into oligos after a possible UVC-assisted synthesis of ribose from similar precursor

molecules (43) and a temperature (67) or formamide-catalyzed (68) phosphorylation. A similar stationary state coupling of reaction to diffusion, leading to regions of high concentration of the products, was shown to occur for purely thermal reactions with different activator and inhibitor diffusion rates by Turing (69) and studied more generally as dissipative structures under the framework of CIT theory by Glansdorff and Prigogine (70).

## 4.2 The Kinetic Equations

Nomenclature, chemical formula, and abbreviations for the concentrations of the participating chemical species of the photochemical reaction leading to adenine shown in figure 3, along with their photon absorption and permeability defining properties are given in table 1.

Table 1: Nomenclature, chemical formula, abbreviation in the text and in kinetic equations, position in figure 3, wavelength of peak absorption (within the spectrum of figure 1), molar extinction coefficient at that wavelength, electric dipole moment and topological polar surface area (TPSA), of the molecules involved in the photochemical synthesis of adenine. Values marked with “??” are estimates since no data have been found in the literature.

Name	chemical formula	abbrev. in text	abbrev. in kinetics	Fig. 3	$\lambda_{max}$ nm	$\epsilon$ M <sup>-1</sup> cm <sup>-1</sup>	$\mu$ [D]	TPSA [Å <sup>2</sup> ]
hydrogen cyanide	HCN	HCN	H	1			2.98	23.8
formamide	H <sub>2</sub> N-CHO	formamide	F		220	60 (71; 72)	4.27 (73)	43.1
formimidic acid	H(OH)C=NH	formimidic acid (trans)	Fa		220	60	1.14 (73)	43.1 ??
ammonium formate	NH <sub>4</sub> HCO <sub>2</sub>	ammonium formate	Af				+/-, 2.0 ??	41.1
diaminomaleonitrile	C <sub>4</sub> H <sub>4</sub> N <sub>4</sub>	cis-DAMN (DAMN)	C	2	298	14000 (74)	6.80 (75)	99.6
diaminofumaritrile	C <sub>4</sub> H <sub>4</sub> N <sub>4</sub>	trans-DAMN (DAFN)	T	3	313	8500 (74)	1.49 (75)	99.6
2-amino-3-iminoacrylimidoyl cyanide	C <sub>4</sub> H <sub>4</sub> N <sub>4</sub>	AIAC	J	4	275	9000 (48; 50)	1.49	99.6 ??
4-aminoimidazole-5-carbonitrile	C <sub>4</sub> H <sub>4</sub> N <sub>4</sub>	AICN	I	7	250	10700 (74)	3.67	78.5
4-aminoimidazole-5-carboxamide	C <sub>4</sub> H <sub>6</sub> N <sub>4</sub> O	AICA	L		266 (76)	10700 ??	3.67 ??	97.8
5-(N <sup>1</sup> -formamidinyl)-1H-imidazole-4-carbonitrileamidine	C <sub>5</sub> H <sub>5</sub> N <sub>5</sub>	amidine	Am		250	10700 (77)	6.83 ??	80.5 ??
adenine	C <sub>5</sub> H <sub>5</sub> N <sub>5</sub>	adenine	A	8	260	15040 (78)	6.83 (79)	80.5
hypoxanthine	C <sub>5</sub> H <sub>4</sub> N <sub>4</sub> O	hypoxanthine	Hy		250	12500 (80)	3.16	70.1

Under non-coherent light sources, photochemical reactions can be treated using elementary kinetics equations of the balance type in the product and reactant concentrations. The following chemical and photochemical reactions must occur in the dissipative structuring of adenine and are described in detail below.

Table 2: Reactions involved in the photochemical synthesis of adenine (see figure 3). Temperature  $T$  is in °K and pH is 7.0 except where noted differently.

#	reaction	reaction constants
1	$\text{H} + \text{H}_2\text{O} \xrightarrow{k_1} \text{F}$	$k_1 = \exp(-14039.0/T + 24.732)$ ; $\text{s}^{-1}$ ; hydrolysis of HCN (50; 81; 82)
2	$\gamma_{220} + \text{F} \rightarrow \text{Fa}$	$q_2 = 0.05$ (71; 72) (83; 84; 85)
3	$\gamma_{220} + \text{Fa} \rightarrow \text{H} + \text{H}_2\text{O}$	$q_3 = 0.03$ (85; 84; 86)
4	$\text{F} + \text{H}_2\text{O} \xrightarrow{k_4} \text{Af}$	$k_4 = \exp(-13587.0/T + 23.735)$ ; $\text{s}^{-1}$ ; hydrolysis of formamide (82; 85)
5	$4\text{H} \xrightarrow{k_5} \text{C}$	$k_5 = (1.0/1.0) \exp(-9964.3/T + 19.049)$ ; $\text{M}^{-1} \text{s}^{-1}$ ; pH 8.2 (50)
6	$4\text{H} \xrightarrow{k_6} \text{T}$	$k_6 = \exp(-\Delta E/RT)/(1. - \exp(\Delta E/RT)) \cdot k_5$ ; $\text{M}^{-1} \text{s}^{-1}$ ; $\Delta E = 0.61 \text{ kcal mol}^{-1}$ (50)
7	$4\text{H} + \text{T} \xrightarrow{k_7} \text{C} + \text{T}$	$k_7 = (1.0/(1.0 \cdot 0.01)) \exp(-(9964.3 - 728.45)/T + 19.049)$ ; $\text{M}^{-2} \text{s}^{-1}$ (50)
8	$4\text{H} + \text{T} \xrightarrow{k_8} 2\text{T}$	$k_8 = k_7$ ; $\text{M}^{-2} \text{s}^{-1}$ (50)
9	$\gamma_{298} + \text{C} \rightarrow \text{T}$	$q_9 = 0.045$ (74)
10	$\gamma_{313} + \text{T} \rightarrow \text{J}$	$q_{10} = 0.058$ (74; 48; 50)
11	$\gamma_{275} + \text{J} \rightarrow \text{I}$	$q_{11} = 0.058$ ; $\text{T} \rightarrow \text{I}$ ; $q_{10} \times q_{11} = 0.0034$ (48; 50)
12	$\text{I} \xrightarrow{k_{12}} \text{L}$	$k_{12} = \exp(-10028./T + 12.974)$ ; $\text{s}^{-1}$ ; $E_a = 19.93 \text{ kcal mol}^{-1}$ (51)
13	$\text{I}:\text{F} + \text{Af} \xrightarrow{k_{13}} \text{A} + \text{F}$	$k_{13} = \exp(-E_a/RT + 12.973)$ ; $\text{M}^{-1} \text{s}^{-1}$ ; $E_a = 6.68 \text{ kcal mol}^{-1}$ (87; 88)
14	$\text{I}:\text{F} + \text{Fa} \xrightarrow{k_{14}} \text{Am} + \text{Fa} + \text{H}_2\text{O}$	$k_{14} = \exp(-E_a/RT + 12.613)$ ; $\text{M}^{-1} \text{s}^{-1}$ ; $E_a = 19.9 \text{ kcal mol}^{-1}$ (89)
15	$\gamma_{250} + \text{Am} \rightarrow \text{A}$	$q_{15} = 0.06$ (77)
16	$\text{A} \xrightarrow{k_{16}} \text{Hy}$	$k_{16} = 10^{(-5902/T + 8.15)}$ ; $\text{s}^{-1}$ ; valid for pH from 5 to 8 (90; 91)
17	$\gamma_{298} + \text{C} \rightarrow \text{C}$	$q_{16} = 0.955$
18	$\gamma_{313} + \text{T} \rightarrow \text{T}$	$q_{17} = 0.942$
19	$\gamma_{275} + \text{J} \rightarrow \text{J}$	$q_{18} = 0.942$
20	$\gamma_{250} + \text{Am} \rightarrow \text{J}$	$q_{19} = 0.940$
21	$\gamma_{250} + \text{I} \rightarrow \text{I}$	$q_{20} = 1.000$
22	$\gamma_{266} + \text{L} \rightarrow \text{L}$	$q_{21} = 1.000$
23	$\gamma_{260} + \text{A} \rightarrow \text{A}$	$q_{22} = 1.000$
24	$\gamma_{250} + \text{Hy} \rightarrow \text{Hy}$	$q_{23} = 1.000$

The following is a detailed description of each reaction given in table 2:

1. Hydrogen cyanide HCN (H) hydrolysis to formamide  $\text{H}_2\text{NCOH}$  (F) with a half-life dependent on temperature and pH (50). The temperature dependent rate equation used here was determined by Kua and Thrush (82) at pH 7.0 from the experimental data of Miyakawa et al. (81).
2. Formamide (F) can be photochemically converted through a photon-induced tautomerization into formimidic acid (Fa). Basch et al. (72) have measured the electronic excitation spectrum of formamide (F) and find a peak in absorption at  $55,000 \text{ cm}^{-1}$  (182 nm) with a molar extinction of  $11,000 \text{ M}^{-1} \text{ cm}^{-1}$ . However, a shoulder exists on the main absorption peak which extends down to  $40,000 \text{ cm}^{-1}$  (250 nm). Duvernay et al. (84) suggest that this shoulder arises from the resonant excitation of the forbidden  $n \rightarrow \pi^*$  transition located at 219 nm ( $130 \text{ kcal mol}^{-1}$ ) and not from the main  $\pi \rightarrow \pi^*$  transition located at 182 nm. Maier and Endres (83) have determined that irradiation of formamide (F) at 248 nm rapidly converts it into basically two tautomeric isomers of formimidic acid (Fa),  $\text{H}(\text{OH})\text{C}=\text{NH}$ , which are both about  $3.6 \text{ kcal mol}^{-1}$  in energy above formamide and separated from it by a transition barrier of height of  $E_a = 45.4 \text{ kcal mol}^{-1}$  (gas phase). Similarly, Duvernay et al. (84) have shown that under UVC light of 240 nm, formamide (F) tautomerizes into formimidic acid (Fa) and their calculation gives a similar transition state barrier height of  $47.8 \text{ kcal mol}^{-1}$ . Wang et al. calculate a transition state barrier of  $49.8 \text{ kcal mol}^{-1}$  (92) but show that this is reduced to  $22.6 \text{ kcal mol}^{-1}$  in the presence of only a single solvent water molecule. This energy needed to overcome the barrier is in the infrared (1265 nm) but Cataldo et al. have shown that there is no evidence of thermal excitation until about  $220 \text{ }^\circ\text{C}$  (93). Our scenario therefore assumes that the  $\text{F} \rightarrow \text{Fa}$  tautomerization requires the absorption of a photon and we take the wavelength region for tautomerization due to the  $n \rightarrow \pi^*$  transition of  $220 \pm 10 \text{ nm}$  and assign an average molar extinction coefficient to that region of  $60 \text{ M}^{-1} \text{ cm}^{-1}$  as measured by Basch et al. (72) and also by Petersen et al. (71).

3. Duvernay et al. (84) have shown that formimidic acid (Fa) can, in turn, be photo-lysed into HCN (H), or HNC, plus H<sub>2</sub>O (dehydration) with maximal efficiency at about 198 nm (86). However, the absorption spectrum of formimidic acid also has a shoulder extending to about 250 nm due to the same  $n \rightarrow \pi^*$  excitation as in formamide. For example, Duvernay et al. observe a small amount of dehydration of formimidic acid at 240 nm. Given that our surface solar spectrum during the Archean (figure 1) is extinguished below about 205 nm, here we likewise assume an absorption wavelength for photo-lysing of  $220 \pm 20$  nm and a similar average molar extinction coefficient as for the tautomerization of fomamide (F) of  $60 \text{ M}^{-1} \text{ cm}^{-1}$  which is in accordance with what Gingell et al. (86) find. Combining photo-reactions #2 and #3, we thus recuperate some of the HCN lost to thermal hydrolysis as described in reaction #1 (see figure 5). Barks et al. (85) have shown that if neat formamide is heated (130 °C), thereby exciting vibrational states, a photon-induced excitation at even longer wavelengths (254 nm) also leads to the formation of HCN with H<sub>2</sub>O, eventually leading to the purines, adenine, guanine, and hypoxanthine, and these yields are increased when including the inorganic catalysts sodium pyrophosphate and calcium carbonate, indicating that heating and inorganic catalysts can improve the photochemical reaction steps #2 and #3. Formamide can also disintegrate thermally into HCN and H<sub>2</sub>O without requiring the absorption of a photon, but only at temperatures greater than about 220 °C (93).

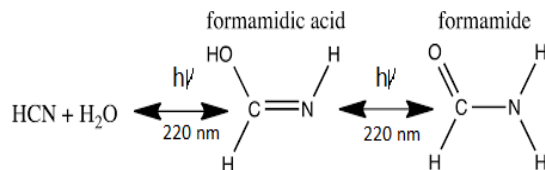


Figure 5: The production of formamimidic acid (Fa) from formamide (F) (photoreaction #2) and its subsequent decay into HCN (H) and water (photoreaction #3). Adapted from Kua and Thrush (82), reprinted with permission.

4. Formamide (F) hydrolyzes to ammonium formate (Af) at a rate of 1% in 24 hr at 100°C (85). The temperature dependent rate equation given in table 2 was determined by Kua and Thrush (82) at pH 7.0 from the experimental data of Miyakawa et al. (81). Ammonium and formate from this salt become useful for the thermal reaction leading to the final addition of an HCN (H) to AICN (I) catalyzed by formamide to give adenine (A) (reaction #13) (87; 88).
5. HCN (H) thermally polymerizes into (HCN)<sub>x</sub> with its most stable tetramer ( $x = 4$ ) known as cis-DAMN (C) being the preferred polymer from which more complex polymers can be synthesized (93). The tetramerization of 4HCN is an exothermic thermal reaction and occurs most rapidly at a solvent pH at its pKa value, which decreases with increasing temperature (pKa = 8.5 at 60 °C and 7.9 at 100°C) (50). The tetramerization of HCN into DAMN is not elementary but involves successive polymerization of HCN with H<sup>+</sup> and CN<sup>-</sup> ions (50) so is second order in the concentration of HCN. The temperature dependence of the rate of conversion of HCN to DAMN has been measured by Sanchez et al. (50). We assume transition state theory and an Arrhenius equation of form,

$$k_5 = \exp(-E_a/RT + \ln A). \quad (5)$$

From the conversion rates for a 1 M solution of HCN with 0.01 M tetramer catalyst as given in table 5 of Sanchez et al. (50) a straight line can be fitted to the graph of  $\ln(1/T)$  vs  $\ln(k_5)$  giving values of  $\ln A = 19.049$  and  $E_a/R = 9964.3$ , or  $E_a = 19.8 \text{ kcal mol}^{-1}$ . However, this would be the rate equation for tetramerization of HCN at its pKa value which would be about 8.2 at 80 °C. At the lower pH value assumed here of 7.0, a somewhat lower rate would be indicated (50).

The rates for hydrolysis and polymerization are similar for concentrations of HCN (H) between approximately 0.01 M and 0.1 M (equal rates at 0.03 M for pH 7, T=80 °, Fig. 15 of reference (50)). At lower concentrations, hydrolysis dominates while at higher concentrations polymerization dominates (50).

6. HCN (H) can also thermally polymerize into trans-DAMN (T) which has a free energy about  $0.56 \text{ kcal mol}^{-1}$  higher than cis-DAMN (C) (75). We therefore assume that the rate constant for the polymerization into trans-DAMN is the same as that for cis-DAMN multiplied by a temperature dependent Boltzmann factor.
7. Trans-diaminomaleonitrile, trans-DAMN (T), produced through the thermal reaction #6 or through the UV photon-induced transformation of cis-DAMN (C) into trans-DAMN (see reaction #9), is a good catalyst because it has electronic donor parts ( $-\text{NH}_2$  groups) and acceptor parts ( $-\text{CN}$  group) linked by a double

bond. As such, it can act as a catalyst for the tetramerization of 4HCN into cis-DAMN (51). Cis-DAMN is also a catalyst for the same thermal reactions, but has significantly less activity than trans-DAMN (50) and therefore its catalytic activity is neglected in our analysis. As can be surmised from the discussion of table 7 of reference (50), including 0.01 M of the tetramer trans-DAMN increases the rate of tetramerization by a factor of 12 at 20 °C which would correspond to a reduction in the activation energy of 1.45 kcal mol<sup>-1</sup>. This change in the barrier height is therefore included in the rate constant for this catalyzed reaction.

8. Trans-DAMN also acts as an auto-catalyst for its own thermal production from 4HCN (51) and we assume a similar reduction in barrier height.
9. cis-DAMN can transform into trans-DAMN (3), step (2) → (3) of figure 3 through a rotation around the double covalent carbon-carbon bond and as such requires the absorption of a high energy photon (298 nm) to overcome the large energy barrier for rotation, calculated to be 58.03 kcal mol<sup>-1</sup> (75) and > 4 eV (48). The quantum yield has been measured by Koch and Rodehorst to be 0.045 (74).
10. The absorption of a photon at 313 nm excites trans-DAMN which then transforms into AIAC through proton transfer from one of the amino groups (48). Although there does not appear to exist a quantum yield for this photochemical reaction in the literature, the quantum yield for trans-DAMN to AICN (T→I) has been measured by Koch and Rodehorst (74) to be 0.0034. We therefore take the quantum yield of both trans-DAMN to AIAC (T→J) and AIAC to AICN (J→I) (reaction # 11) to be equal to  $\sqrt{0.0034}$ .
11. AIAC (J) on absorbing a photon at 275 nm then transforms through photon-induced cyclicization (ring closure) into an azetene intermediate (5 of figure 3) in an excited state, which then transforms to the N-heterocyclic carbene (6 of figure 3) and finally this tautomerizes to give the imidazole AICN (I) (48). As noted above, the quantum yield for this process (J→I) is taken to be  $\sqrt{0.0034}$  to give the overall quantum yield for trans-DAMN to AICN (T→I) to be 0.0034 (74). AICN absorbs maximally at wavelength 250 nm.
12. The imidazole, 4-aminoimidazole-5-carbonitrile, AICN (I) created in the previous photochemical reaction (reaction # 11) can hydrolyze to 4-aminoimidazole-5-carboxamide, AICA (L). We determined the rate equation for this 1st order reaction from the data of Sanchez et al. (51) at different temperatures (their table 1). From this temperature data, we determined the barrier to hydrolysis to be 19.93 kcal mol<sup>-1</sup> and the frequency factor to be  $\ln A = 12.974$ .
13. The final coupling of a fourth HCN to AICN (I) and its cyclization to form adenine (A) is a very exothermal overall,  $\Delta G = -53.7$  kcal mol<sup>-1</sup>, but there are numerous large energy barriers on the path to its completion (52). The first step is the coupling of an HCN molecule to AICN, and this appears to be rate limiting since it has the highest energy barrier, calculated in the gas phase, of 39.7 kcal mol<sup>-1</sup> (52). However, it is catalyzed by both bulk solvent and specific water molecules which reduce the barrier to 29.6 kcal mol<sup>-1</sup>, or by ammonium molecules with bulk water solvent which reduce the barrier further to 27.6 kcal mol<sup>-1</sup> (52). A number of experimental works (87; 88; 94; 85) have revealed that ammonium formate (Af) could provide a route with an even lower barrier, but the rate is still too slow to allow significant adenine production from AICN and ammonium formate, unless a strong concentration mechanism existed, for example, dehydration (85), or perhaps the build up of concentration inside the vesicle, or the reaction-diffusion self-organizing occurring within the vesicle, as suggested here.

However, as early as 1974 Yonemitsu et al. (87) showed that including formamide, the hydrolysis product of HCN (reaction #1), in aqueous solution, or by itself (neat solution), along with ammonium formate could dramatically speed up the reaction as long as the temperature was above approximately 80 °C, leading to a proposal for an industrial patent for the production of adenine from cis-DAMN (C) or trans DAMN (T) and formamide with ammonium formate. From examples 1 and 12 of the experiments of Yonemitsu et al. carried out at 150 and 100 °C (using 135 g of formamide, 30 g of ammonium formate, and 2.01 g of DAMN) giving rise to 43.5% and 30.0% product of adenine after 5 and 10 hours at those temperatures respectively, it is possible to calculate an activation barrier for the overall reaction of  $E_a = 6.682$  kcal mol<sup>-1</sup>. Since ammonium formate is a salt, the probable pathway from AICN to adenine would be that proposed by Zubay and Mui (88) where the ammonium ion NH<sub>4</sub><sup>+</sup> attacks the triple NC bond of AICN and the formate ion HCOO<sup>-</sup> attacks the amine NH<sub>2</sub> group of AICN (figure 8 of reference (88)) both catalyzed by the proton transfer process involving formamide (see below), leading to this very low barrier. We therefore assume the reaction to be of second order and determined by the Arrhenius equation of form,

$$k_{13} = \exp(-E_a/RT + \ln A), \quad (6)$$

where  $E_a = 6.682 \text{ kcal mol}^{-1}$  and the pre-exponential frequency factor  $A$  was estimated from the reduced mass dependence of the Langevin model (95),  $A = 2\pi e\sqrt{\alpha/\mu}$  for a charged ion - neutral molecule system where  $e$  is the ion electronic charge,  $\alpha$  is the polarizability of the neutral reactant, and  $\mu$  is the reduced mass of the reactants (96). Considering that all factors are equal except the reduced mass and then normalizing to the frequency factor of reaction #12 for the hydrolysis of AICN (I) by the inverse square root of the reduced mass for the reacting species, gives a value of  $\ln A = 12.9734$ .

14. There exists a second possible route to adenine from AICN and HCN, without involving ammonium formate but considering the catalytic effect of formamide. Recently, Wang et al. (89) have studied through *ab initio* DFT calculations the synthesis of adenine starting from only formamide and propose what they call a “formamide self-catalytic mechanism”. This mechanism consists of (1) a proton transfer from N to O of formamide to form the imidic acid tautomer, formimidic acid (Fa), obtained in our case through photon-induced proton transfer reaction #2); (2) a proton exchange between one imidic tautomer and one amide tautomer, resulting in two formimidic acids; and (3) an interaction between these two imidic acids yielding formimidic acid, a water molecule, and HCN. This formamide self-catalytic mechanism has relevance to the entire adenine synthesis process starting from only formamide since it reduces many of the barriers on route to adenine (89).

Of Wang et al.’s results, what is important to us here, therefore, is the step of the attachment of HCN to the amine group ( $\text{NH}_2$ ) of AICN. They show for their particular case of formiminylation of 5-aminoimidazole (Fig. 13 of reference (89)) that this reaction can be formamide-catalyzed (as described above) and find the activation energy barrier for this to be  $19.9 \text{ kcal mol}^{-1}$  (significantly lower than  $46.1 \text{ kcal mol}^{-1}$  in the noncatalyzed process and  $34.0 \text{ kcal mol}^{-1}$  in the water-assisted process) and that the subsequent dehydration process to give the amidine (Am) (our case) is calculated to be  $14.0 \text{ kcal mol}^{-1}$  ( $34.3 \text{ kcal mol}^{-1}$  in the noncatalyzed reaction).

Therefore, we assume that the attachment of HCN (H) to AICN (I) to form 5-(N'-formamidinyl)-1H-imidazole-4-carbonitrileamidine (Am) to be a formamide catalyzed thermal reaction involving formimidic acid and formamide and we assume the rate of this reaction to be determined by the Arrhenius equation of form

$$k_{14} = \exp(-E_a/RT + \ln A) \quad (7)$$

where  $E_a = 19.9 \text{ kcal mol}^{-1}$  and the pre-exponential frequency factor  $A$  is again estimated from the reduced mass dependence of the Langevin model (95), considering again all factors equal except the reduced mass and then normalizing to the reaction #12 for the hydrolysis of AICN (I) by the inverse square root of the reduced mass for the reacting species, giving a value of  $\ln A = 12.613$ .

It is important to note that AICN (I) has a conical intersection for a charge transfer from the molecule in the excited state to a neighboring cluster of water molecules (97). With AICN left in the charged state, this would significantly increase the rate of attachment through charge-dipole interaction to formamide, which has a dipole moment significantly larger than that of water (table 1), effectively changing the reaction from third order to second order, thereby increasing significantly the overall rate of this last attachment of HCN to AICN through this formamide catalyzed reaction.

The possibility of hot ground state reaction occurring to aid in overcoming the barrier to producing adenine from AICN (I) and HCN (H) should also be considered during daylight periods. These could occur within a narrow time window after photon excitation, calculated by Boulanger et al. for a molecule (trans-DAMN) which has a similar conical intersection as AICN, to be about 0.2 ps, which corresponds to the time at which the excess energy on the molecule has been reduced to about 1/3 of its initial value, allowing reactions to proceed with a maximum barrier height of about  $30 \text{ kcal mol}^{-1}$  (48). This possibility will not be included in our model, but it would have the effect of increasing the rate of the production of adenine.

15. After the attachment of a fifth HCN (H) to AICN (I) to form the amidine (Am), reaction #14, a subsequent tautomerization is required (calculated to have a high barrier of about  $50 \text{ kcal mol}^{-1}$ ) which, once overcome, allows the system to proceed through a subsequent barrier-less cyclicization to form adenine (77). Such a high barrier to the final cyclicization means that, for the temperatures considered here, it cannot be a thermal reaction. The fact that adenine has been found in space and in meteorites where temperatures are expected to be very low indicated to Glaser et al. (77) that a photochemical route must be available. They suggested a photon-induced tautomerization with the amidine which absorbs strongly at 250 nm. Although oscillator strengths for the tautomerization have been calculated by Glaser et al., different *ab initio* approaches give significantly different values and experiment will be required for its reliable determination. Therefore, until

such data becomes available, we assume a similar molar extinction coefficient as for AICN and a quantum efficiency of  $q_{15} = 0.06$ , the latter being of the same order as the other photochemical reactions listed here.

16. The temperature dependent rate equation for the removal of adenine (A) through hydrolysis to give hypoxanthine (Hy) which could then lead to guanine, or through deamination to some amino acids (98) was determined by Levy and Miller (90), and also by Wang and Hu (91). Zheng and Meng calculated a transition state barrier of  $23.4 \text{ kcal mol}^{-1}$  (99).
17. to 24. These reactions represent the absorption of a photon in a 20 nm region around the wavelength of peak absorption of the molecule which then decays through internal conversion at a conical intersection to the ground state on sub-picosecond time scales. All molecules listed in this set of photo-reactions are basically photo-stable, having a peaked conical intersection of the excited state with the ground state. These reactions, with large quantum efficiencies, represent the bulk of the flow of energy from the incident UVC spectrum to the emitted outgoing ocean surface spectrum in the infrared and therefore contribute most to dissipation and entropy production.

The autocatalytic nature of trans-DAMN (T) and formamide (F) in aiding in the thermal reactions, particularly in the polymerization of HCN (table 7 of reference (50)), lead to its proliferation, and therefore also the proliferation of the final product adenine under the continuous UVC flux. The final product, adenine (8), has the greatest molar extinction and dissipative efficacy of all the intermediate precursor molecules of figure 3 within the UVC region arriving at Archean Earth’s surface (figure 1). Inorganic catalysts have not been included directly in our reaction scheme. It has been shown, however, that inorganic catalysts increase the rate of adenine production, for example  $\text{Cu}^{+2}$  ions have a large effect in increasing the rate constant for the conversion of HCN (H) to cis-DAMN (C) (50).  $\text{Cu}^{+2}$  ions also reduce the energy difference between the isomers (but not the barrier crossing height) formimidic and formamidic acid of formamide (100). Metal ions would have been in high abundance at the ocean surface microlayer (58; 59).

In order to obtain simple kinetic equations for the photochemical reactions, we assume that the molecules only absorb within a region  $\pm 10 \text{ nm}$  of their maximum absorption wavelength  $\lambda_{max}$  and that this absorption is at their maximum molar extinction with coefficient  $\epsilon$  (table 1), and finally that these wavelength regions do not overlap. We assume that the vesicle is at the ocean surface and the depth coordinate is divided into  $i = 20$  bins of width  $\Delta x = 5 \mu\text{m}$  and the time interval for the recursion calculation for the concentrations at a particular depth is 5 ms. The recursion relation for the factor of light intensity  $L_\lambda(i)$  at a distance  $x(i) = i \cdot \Delta x$  below the ocean surface will be,

$$L_\lambda(i, C(i)) = L_\lambda(i - 1, C(i - 1))e^{-\Delta x \cdot \alpha_\lambda} \cdot 10^{-\Delta x \cdot \epsilon_\lambda C(i)} \quad (8)$$

where  $\alpha_\lambda$  is the absorption coefficient of water at wavelength  $\lambda$  and  $\epsilon_\lambda$  is the molar extinction coefficient of the particular absorbing substance which has concentration  $C(i)$  at  $x(i)$ .

The kinetic equation recursion relations for a time step  $dt$  and a depth bin of width  $\Delta x$  at a distance  $x$  below

the surface are determined from reactions of table 2 to be the following;

$$\begin{aligned}\frac{dH}{dt} &= D_H \frac{\partial^2 H}{\partial x^2} - k_1 H + d \cdot q_3 I_{220} L_{220}(Fa) \frac{(1 - 10^{-\Delta x \epsilon_{220} Fa})}{\Delta x} - k_5 H^2 - k_6 H^2 - k_7 H^2 T - k_8 H^2 T \\ &= D_H \frac{\partial^2 H}{\partial x^2} + d \cdot q_3 I_{220} L_{220}(Fa) \frac{(1 - 10^{-\Delta x \epsilon_{220} Fa})}{\Delta x} - H k_1 - H^2 (k_5 + k_6 + T(k_7 + k_8))\end{aligned}\quad (9)$$

$$\frac{dF}{dt} = D_F \frac{\partial^2 F}{\partial x^2} + k_1 H - d \cdot q_2 I_{220} L_{220}(F) \frac{(1 - 10^{-\Delta x \epsilon_{220} F})}{\Delta x} - k_4 F - k_{14} I F a \quad (10)$$

$$\frac{dFa}{dt} = D_{Fa} \frac{\partial^2 Fa}{\partial x^2} + d \cdot q_2 I_{220} L_{220}(F) \frac{(1 - 10^{-\Delta x \epsilon_{220} F})}{\Delta x} - d \cdot q_3 I_{220} L_{220}(Fa) \frac{(1 - 10^{-\Delta x \epsilon_{220} Fa})}{\Delta x} \quad (11)$$

$$\frac{dAf}{dt} = D_{Af} \frac{\partial^2 Af}{\partial x^2} + k_4 F - k_{13} I A f \quad (12)$$

$$\frac{dC}{dt} = D_C \frac{\partial^2 C}{\partial x^2} + k_5 H^2 + k_7 H^2 T - d \cdot q_9 I_{298} L_{298}(C) \frac{(1 - 10^{-\Delta x \epsilon_{298} C})}{\Delta x} \quad (13)$$

$$\frac{dT}{dt} = D_T \frac{\partial^2 T}{\partial x^2} + k_6 H^2 + k_8 H^2 T + d \cdot q_9 I_{298} L_{298}(C) \frac{(1 - 10^{-\Delta x \epsilon_{298} C})}{\Delta x} - d \cdot q_{10} I_{313} L_{313}(T) \frac{(1 - 10^{-\Delta x \epsilon_{313} T})}{\Delta x} \quad (14)$$

$$\frac{dJ}{dt} = D_J \frac{\partial^2 J}{\partial x^2} + d \cdot q_{10} I_{313} L_{313}(T) \frac{(1 - 10^{-\Delta x \epsilon_{313} T})}{\Delta x} - d \cdot q_{11} I_{275} L_{275}(J) \frac{(1 - 10^{-\Delta x \epsilon_{275} J})}{\Delta x} \quad (15)$$

$$\frac{dI}{dt} = D_I \frac{\partial^2 I}{\partial x^2} + d \cdot q_{11} I_{275} L_{275}(J) \frac{(1 - 10^{-\Delta x \epsilon_{275} J})}{\Delta x} - k_{12} I - k_{13} I A f - k_{14} I F a \quad (16)$$

$$\frac{dL}{dt} = D_L \frac{\partial^2 L}{\partial x^2} + k_{12} I \quad (17)$$

$$\frac{dAm}{dt} = D_{Am} \frac{\partial^2 Am}{\partial x^2} + k_{14} I F a - d \cdot q_{15} I_{250} L_{250}(Am) \frac{(1 - 10^{-\Delta x \epsilon_{250} Am})}{\Delta x} \quad (18)$$

$$\frac{dA}{dt} = D_A \frac{\partial^2 A}{\partial x^2} + d \cdot q_{15} I_{250} L_{250}(Am) \frac{(1 - 10^{-\Delta x \epsilon_{250} Am})}{\Delta x} + k_{13} I A f - k_{16} A \quad (19)$$

$$\frac{dHy}{dt} = D_{Hy} \frac{\partial^2 Hy}{\partial x^2} + k_{16} A \quad (20)$$

where  $d$  is the day/night factor, equal to 1 during the day and 0 at night.  $I_{220}, I_{298}, I_{313}, I_{275}$  and  $I_{250}$  are the intensities of the photon fluxes at 220, 298, 313, 275 and 250 nm respectively (Fig. 1).  $\epsilon_\lambda$  are the coefficients of molar absorption for the relevant molecule and  $\alpha_\lambda$  are the water absorption coefficients at the corresponding photon wavelengths  $\lambda$ , respectively.

### 4.3 Vesicle Permeability and Internal Diffusion

The permeability of the molecule through the vesicle wall and the diffusion constant of the molecule within the inner aqueous region of the vesicle will both decrease with the area of the molecule and with the size of its electric dipole moment (table 1) and increase with temperature. It is interesting to note that almost all of the final and intermediate product molecules have large dipole moments, implying their entrapment within the vesicle. We assume that the vesicle cannot remain intact at temperatures greater than 90 °C but that below this temperature it is completely permeable to H<sub>2</sub>O, HCN (H) and formimidic acid (Fa) but impermeable to all the other products due to their large size and large electric dipole moments. Note that ammonium formate would be in its ionic form and therefore also unable to cross the fatty acid membrane. Permeabilities across lipid boundaries are reduced by orders of magnitude if the molecules are polar or are charged (101).

The diffusion constant  $D_Y$  for the molecule  $Y$  will depend on the viscosity of the liquid inside the vesicle, or, in other words, on amount of organic material built up through UVC dissipative structuring within the vesicle from the precursor molecules HCN and H<sub>2</sub>O. Studies of intracellular diffusion of nucleotides indicate three factors influencing diffusion rates besides temperature at high solute densities; the viscosity of the environment, collisional interactions dependent on concentration, and binding interactions between molecules (102). The diffusion constant of adenine in pure water has been determined to be  $D_A = 7.2 \times 10^{-6} \text{ cm}^2 \text{ s}^{-1}$  (103) while the measured diffusion rates in the cytoplasm of different cell types has been measured to be between  $1.36 \times 10^{-6}$  to  $7.8 \times 10^{-6} \text{ cm}^2 \text{ s}^{-1}$  (102).

It seems likely, therefore, that, at least in some areas of the primitive ocean, there would have existed surface films with a high density of trace metals, lipids and fatty acids and other hydrocarbons produced, for example, by

the same ultraviolet spectrum of figure 1 on CO<sub>2</sub> saturated water (14). Diffusion in the sea surface microlayer could then be expected to be orders of magnitude lower than in the bulk water.

Diffusion rates in our case will depend on the amount of organic material already existing at the air/water surface captured during the formation of the vesicle, which may vary considerably. We define all diffusion constants relative to adenine through the formula;

$$D_Y = \frac{\mu_A A_A}{\mu_Y A_Y} \cdot D_A, \quad (21)$$

where  $A_A$  is the polar surface area of adenine (table 1) and investigate three different scenarios with diffusion constants of three different orders of magnitude around the largest value for the diffusion constant of adenine in present day cytoplasm. Using the values given in table 1 for the dipole moment and the area, we obtain the results given in table 3.

Table 3: Diffusion constant factors for the molecules obtained from equation 21 considering three different scenarios of  $D_A = 1 \times 10^{-5}, 1 \times 10^{-6}$  and  $1 \times 10^{-7} \text{ cm}^2 \text{ s}^{-1}$ .

$D_H$	$D_F$	$D_{Fa}$	$D_{Af}$	$D_C$	$D_T$	$D_J$	$D_I$	$D_L$	$D_{Am}$	$D_A$	$D_{Hy}$
7.752	2.988	11.190	6.689	0.892	4.073	4.073	1.908	1.532	1.000	1.000	2.482

Cyclical boundary conditions are assumed for diffusion, except for HCN (H) and formimidic acid (Fa) which can permeate the vesicle wall and therefore take on their fixed value specified in the initial conditions outside the vesicle (see below). The second order derivatives for the diffusion were calculated using 3 terms with single precision variables.

#### 4.4 Initial Conditions

Miyakawa, Cleaves and Miller (81) estimated the steady state bulk ocean concentration of HCN at the origin of life assuming production through electric discharge on atmospheric methane to produce radicals which attack N<sub>2</sub>, leading to an input rate to the oceans of 100 nmole cm<sup>-2</sup> y<sup>-1</sup>, and loss of HCN to hydrolysis plus a 10 million year recycling time of all ocean water through submarine vents for an ocean of 3 Km average depth. For an ocean of pH 6.5 and 80 °C, they obtained a value of [HCN]=  $1.0 \times 10^{-10}$  M (81).

However, HCN can also be produced through the solar Lyman alpha line (121.6 nm) photo-lysing N<sub>2</sub> in the upper atmosphere giving atomic nitrogen which then combines with CH and CH<sub>2</sub> to give HCN, or through 145 nm photolysis of CH<sub>4</sub> leading to a CH\* radical which attacks N<sub>2</sub> to give HCN (40). Including this UV production would increase the input of HCN concentration to the oceans by a factor of at least 6 (104; 105; 53). The first ~ 100 μm of the ocean surface is a unique region known as the hydrodynamic boundary layer in which surface tension leads to enriched organics with densities up to 10<sup>4</sup> times that of organic material in the water column slightly below (58). Trace metal enhancement in this microlayer can be one to three orders of magnitude greater than in the bulk (58; 106). Langmuir circulation, Eddy currents, and the scavenging action of bubbles tends to concentrate organic materials into this surface film. If disturbed or mixed, the film rapidly reestablishes its integrity. This high density of organic material trapped through hydrophobic and ion interactions at the ocean surface leads to significantly lower rates of diffusion at the surface microlayer as compared to the ocean bulk (58). Little diffusion and turbulence therefore imply little mixing. The ocean microlayer is therefore a very stable layer which, of course, would not be recycled through ocean vents. Finally, although HCN is very soluble in bulk water, recent molecular dynamic simulations have shown that it concentrates to about an order of magnitude larger at the air-water interface due to lateral HCN dipole-dipole interactions, and that it evaporates at lower rates than does water (60).

Therefore, rather than assuming the low bulk concentrations of Miyakawa et al., we instead consider various higher initial surface concentrations for HCN (H) and formimidic acid (Fa), the latter resulting from a photochemical tautomerization of formamide, the hydrolysis product of HCN (reactions #1 and #2 of table 2). We also consider the probable existence of small isolated patches of much higher concentrations, up to  $1.0 \times 10^{-2}$  M of these molecules, due to the above mentioned characteristics of the microlayer. The initial concentrations of all other reactants and products inside the vesicle (assumed impermeable to these) are taken to be  $1.0 \times 10^{-10}$  M.

## 5 Results

In figures 6 through 11 I present the concentrations as a function of time in Archean days (16 hours) of the relevant molecules in the photochemical synthesis of adenine obtained by solving simultaneously the differential kinetic

equations, (9) through (20), for the initial conditions and diffusion constants listed in the figure legend.

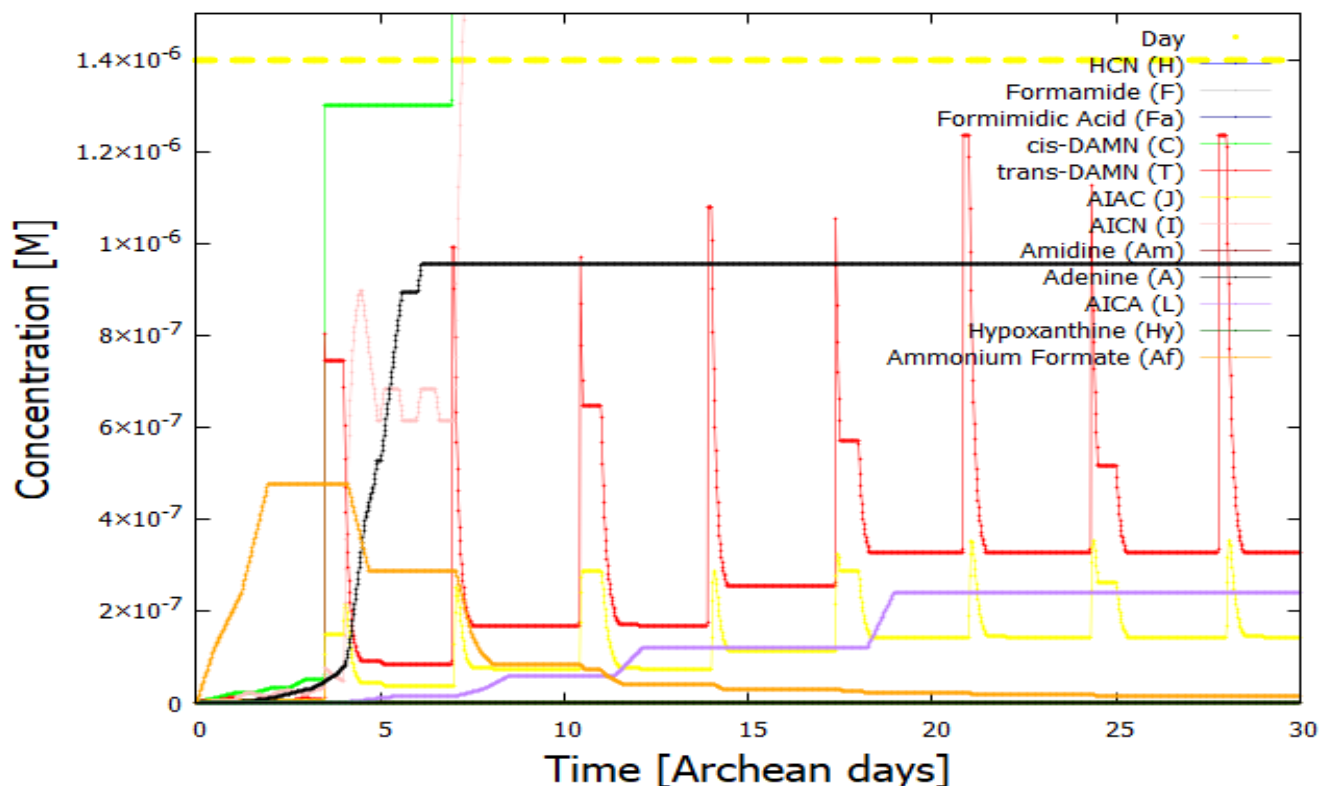


Figure 6: Concentrations as a function of time in Archean days (16 hours) of the molecules dissipatively structured on route to the synthesis of adenine. The initial conditions are;  $T=80\text{ }^{\circ}\text{C}$ ,  $[\text{H}]_0 = 6.0 \times 10^{-5}\text{ M}$ ,  $[\text{F}]_0 = 1.0 \times 10^{-5}\text{ M}$ ,  $[\text{Fa}]_0 = 1.0 \times 10^{-5}\text{ M}$  and all other initial concentrations  $[\ ]_0 = 1.0 \times 10^{-10}\text{ M}$ . The diffusion constant exponential factor was  $expn = 1.0 \times 10^{-6}$  (e.g.  $D_A = 1.0 \times 10^{-6}\text{ cm}^2\text{ s}^{-1}$ ). There were 8 perturbations of the system corresponding to the vesicle floating into regions of higher HCN (H) and formimidic acid (Fa) concentrations of 0.01 M for two minutes every 3.5 Archean days (as evidenced by the vertical spikes in the concentration of trans-DAMN (red line)). The yellow horizontal dashed line represents the alternate periods of daylight (yellow) and night (blank). After one Archean month, the concentration of adenine within the vesicle (black line) has grown by approximately four orders of magnitude, from  $1.0 \times 10^{-10}$  to almost  $1.0 \times 10^{-6}$ .

Figures 13 and 14 plot the concentration profile of the products as a function of depth below the ocean surface for the initial conditions of figure 12 at the time of 7.3 Archean days. The coupling of reaction to diffusion leads to a non-homogeneous distribution of products, with some of these demonstrating a significant increase in concentration towards the center of the vesicle.

In table 4 I list the temperature dependence of the production of the important molecules after a 30 day period for different initial and boundary conditions.

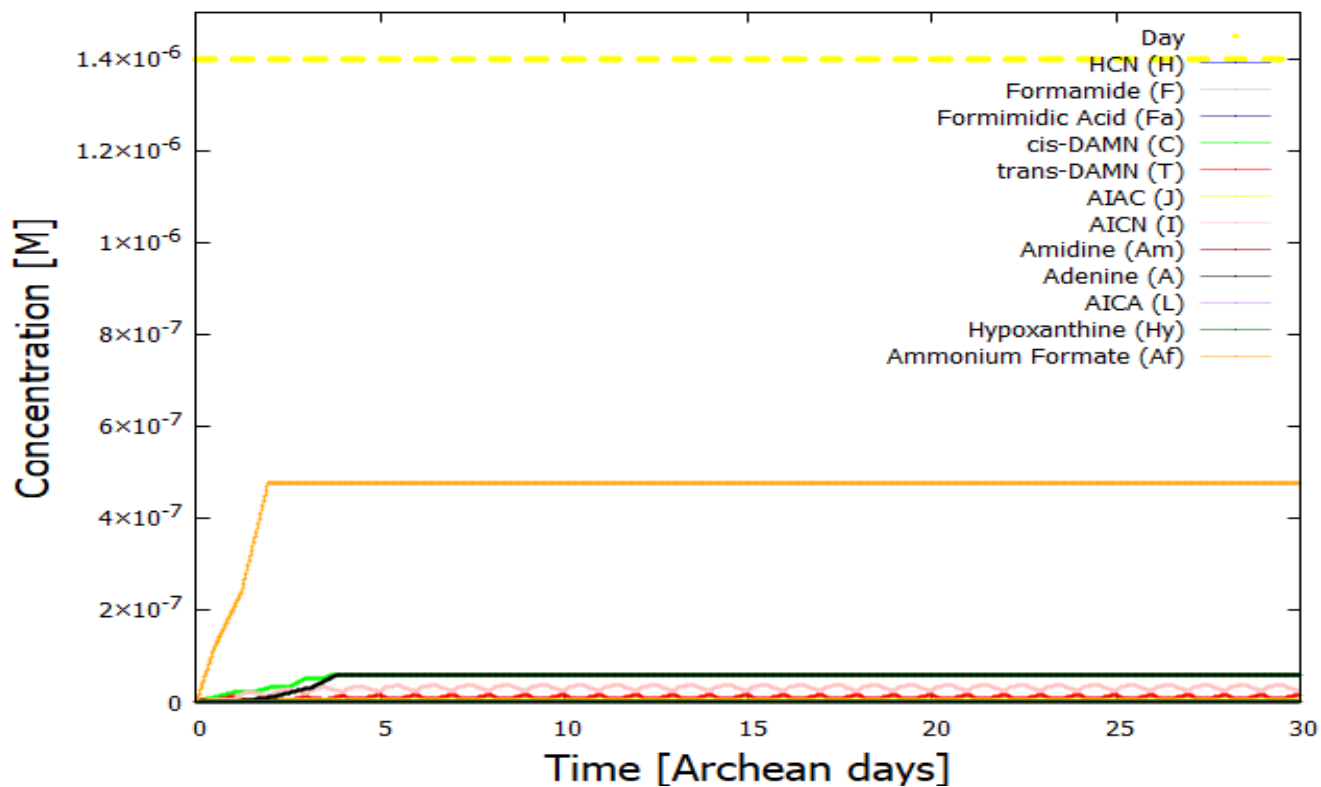


Figure 7: The same as Fig. 6 except with no perturbations of the system, i.e. the system does not encounter patches of higher concentration of HCN and Fa. The concentrations of these molecules are held constant at  $6 \times 10^{-5}$  and  $1 \times 10^{-5}$  M respectively for the 30 day period. The concentration of adenine (black line) only rises to  $5.96 \times 10^{-8}$  M over the 30 day period.

Table 4: Concentrations in moles per liter M of the product molecules obtained at the given temperature and given initial conditions for HCN (H), formamide (F) and formamimidic acid (Fa) after a 30 day period. Those labeled with “perturbation” correspond to the vesicle floating into 8 patches of 0.01 M HCN and Fa for two minutes every 3.5 Archean days.

T °C	F	Fa	Af	C	T	J	I	Am	A	L	Hy
[H]=6E-06, [F]=1E-06, [Fa]=1E-06 M, $D_A = 1.0 \times 10^{-6}$ , perturbation											
80	3.907E-06	1.000E-06	5.504E-09	2.516E-06	1.614E-07	7.190E-08	9.162E-06	1.067E-10	2.384E-07	2.384E-07	1.000E-10
[H]=6E-05, [F]=1E-05, [Fa]=1E-05 M, $D_A = 1.0 \times 10^{-6}$ , perturbation											
60	1.026E-05	1.000E-05	1.708E-08	6.379E-07	3.959E-08	1.438E-08	1.907E-06	1.000E-10	1.192E-07	7.450E-09	1.000E-10
70	1.088E-05	1.000E-05	1.718E-08	1.278E-06	8.223E-08	3.739E-08	3.815E-06	1.012E-10	2.384E-07	2.980E-08	1.000E-10
80	1.282E-05	1.000E-05	1.346E-08	5.076E-06	3.258E-07	1.409E-07	1.216E-05	1.069E-10	9.537E-07	2.384E-07	2.328E-10
90	1.865E-05	1.000E-05	2.136E-08	1.016E-05	6.548E-07	2.905E-07	2.453E-05	1.303E-10	2.564E-06	9.537E-07	1.863E-09
[H]=6E-04, [F]=1E-04, [Fa]=1E-04 M, $D_A = 1.0 \times 10^{-6}$ , perturbation											
80	1.028E-04	1.000E-04	6.027E-08	1.390E-05	1.725E-06	4.861E-07	2.178E-05	1.154E-10	7.629E-06	4.768E-07	1.862E-09
[H]=6E-05, [F]=1E-05, [Fa]=1E-05 M, $D_A = 1.0 \times 10^{-8}$ , perturbation											
80	1.514E-05	1.001E-05	1.263E-08	5.079E-06	3.258E-07	1.409E-07	1.525E-05	1.145E-10	9.537E-07	4.768E-07	2.328E-10
[H]=6E-05, [F]=1E-05, [Fa]=1E-05 M, $D_A = 1.0 \times 10^{-10}$ , perturbation											
80	1.678E-04	1.097E-05	5.386E-09	8.430E-05	5.478E-06	2.41E-06	3.910E-04	2.419E-09	7.629E-06	7.629E-06	1.863E-09
[H]=6E-05, [F]=1E-05, [Fa]=1E-05 M, $D_A = 1.0 \times 10^{-6}$ , no perturbation											
20											
80	1.000E-05	1.000E-05	4.768E-07	5.960E-08	1.578E-08	2.876E-09	2.378E-08	1.000E-10	5.960E-08	9.313E-10	1.000E-10
90	1.000E-05	1.000E-05	9.537E-07	1.192E-07	3.498E-08	5.627E-09	1.376E-08	1.000E-10	2.384E-07	1.863E-09	2.328E-10

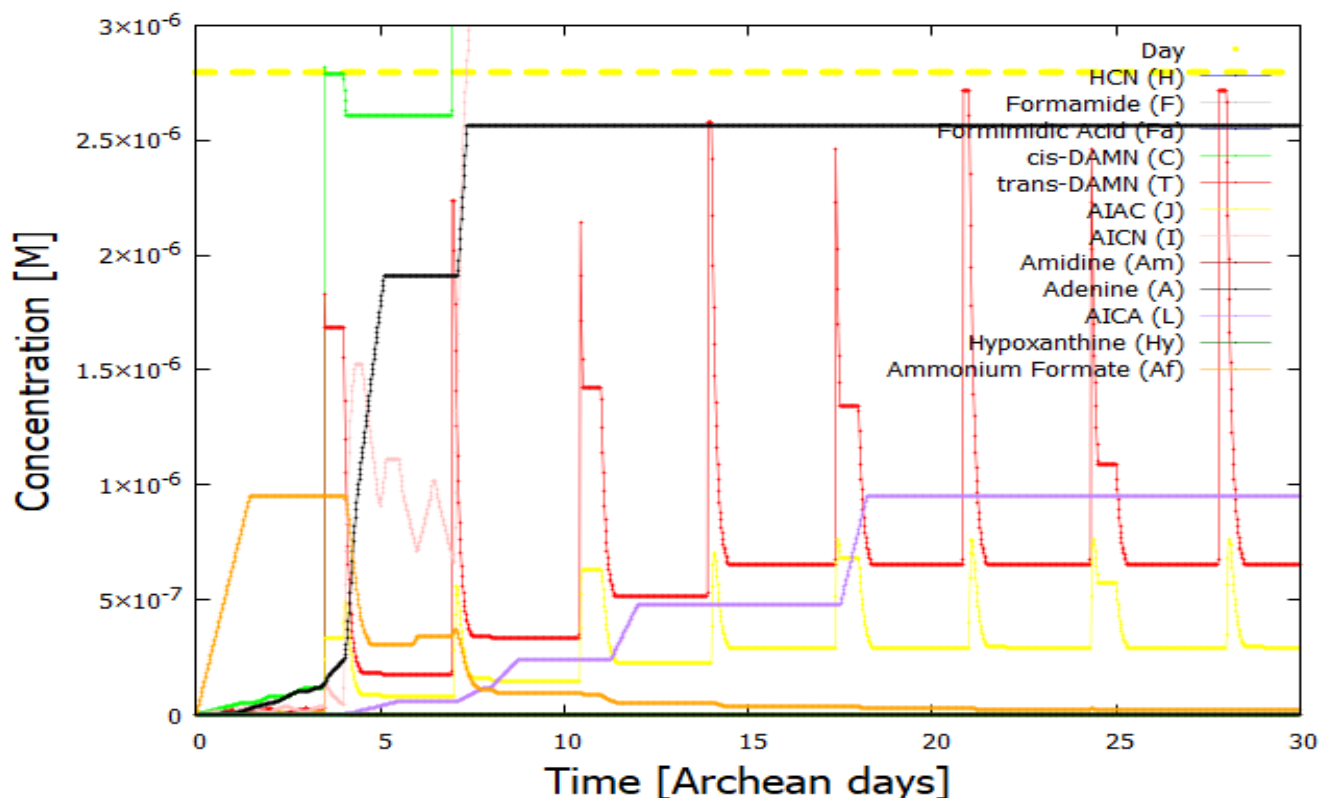


Figure 8: The same as Fig. 6 except for a temperature of 90 °C. All other conditions are identical. The concentration of adenine (black line) rises to  $2.6 \times 10^{-6}$  M over the 30 day period.

The temperature dependence of the concentrations of the product molecules after 30 Archean days is given in figure 15.

In figure 16 I plot the entropy production as a function of time in Archean days due to purely photon dissipation as represented by reactions 17 to 24 of table 2. In general, the entropy production is an increasing function of time. These photo-reactions represent the terms  $d_J P/dt$ , and even though the terms  $d_X P/dt$  which represent the variation of the entropy production due to rearrangement of the affinities, are negative definite (corresponding to the structuring of the molecules) consistent with the Glansdorf-Prigogine universal evolutionary criterion, the total entropy production  $dP/dt = d_J/dt + d_X/dt$  increases due to the fact that, as shown here, the first term which represents the flow of energy through the system being converted from short wavelength into long wavelength light, increases greatly over the evolution of the concentrations of the intermediates in the system of reactions. The product molecules, including adenine, have, in this sense, been dissipatively structured and should be identified as *microscopic dissipative structures*.

In figure 17 I plot the entropy production as a function of time in Archean days due to purely photon dissipation as represented by reactions 17 to 24 of table 2 for the case in which there are no high concentration patches of HCN and Fa on the ocean surface and concentrations are kept constant at  $6 \times 10^{-5}$  and  $1 \times 10^{-5}$  respectively (i.e. no perturbation of the vesicle).

## 6 Discussion

Table 4 and the comparison of figures 6 and 7 clearly indicate that perturbing the system by allowing it to float into regions of high HCN and formimidic acid concentration provokes the system into new stationary states of higher product concentration, particularly for adenine. Table 4 and figure 15 also indicate that high temperatures are important for increasing the rates of the dissipative structuring of adenine. Cold origin of life scenarios were proposed so that eutectic concentration would increase the rate of tetramerization of HCN (H) to cis-DAMN (C) with respect to the rate of hydrolysis of HCN to formamide (F) (reaction #1, table 2). However, formamide and its

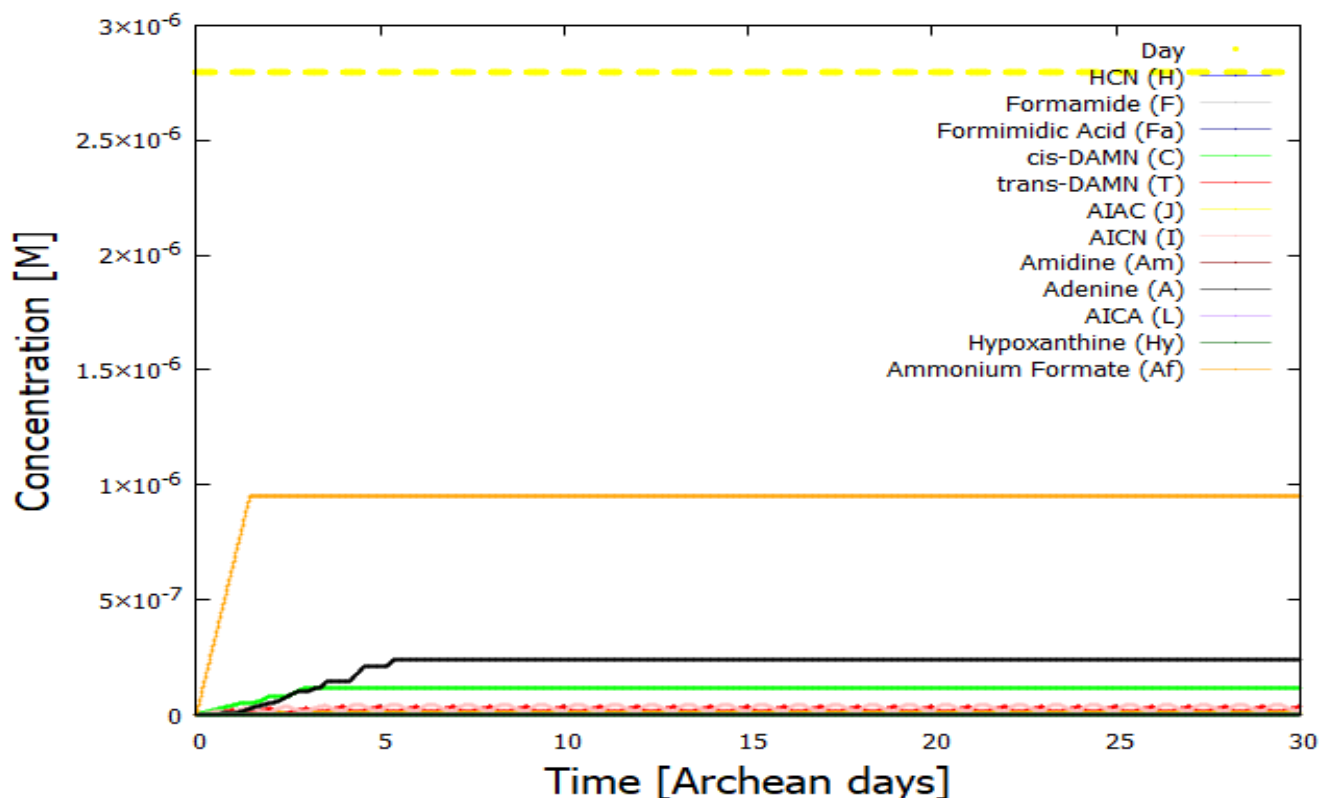


Figure 9: The same as Fig. 8, 90 °C, except with no perturbations of the system, i.e. the system does not encounter patches of HCN and Fa, these concentrations are maintained constant at  $6 \times 10^{-5}$  and  $1 \times 10^{-5}$  M respectively for the whole 30 day period.

hydrolysis product of ammonium formate (Af) are both very important in the final step from AICN (I) to adenine (A) (reactions #13 and #14, table 2). Our vesicle model provides for a build up of product concentrations within the vesicle over time even at high temperatures. Furthermore, phosphorylation can be performed with phosphate salts and formamide which favors the formation of acyclonucleosides and the phosphorylation and trans-phosphorylation of nucleosides and this occurs most rapidly at high temperatures  $\gtrsim 70$  °C (67; 68).

Table 4 shows the final product molecule concentrations after 30 Archean days as a function of the ocean surface concentration of HCN;  $6 \times 10^{-6}$ ,  $6 \times 10^{-5}$ , and  $6 \times 10^{-4}$  M, at 80 °C and different diffusion constant exponentials of  $1 \times 10^{-6}$ ,  $1 \times 10^{-8}$ , and  $1 \times 10^{-10}$ . These concentrations are higher than normally assumed in origin of life scenarios and are justified on the grounds that; 1) it has been discovered that the ocean surface microlayer can have organic densities at  $10^4$  times larger than the bulk, implying a greater viscosity and therefore a much lower diffusion constant for the molecules at the surface, and 2) HCN has a large dipole moment, implying ion-dipole interactions with ions trapped in the surface microlayer. Yet another concentration mechanism for HNC may arise from the coupling between reaction and diffusion in the non-linear regime which leads to the breaking of spatial symmetry (e.g. the Belousov-Zhabotinsky reaction (1)). The homogeneous stationary state may no longer be stable with respect to a space dependent perturbation and intermediate products may become preferentially concentrated, and be consumed, in a given region. We did, in fact, find this for our model, where the largest concentrations occurred at the center of the vesicle, but only significant for very low diffusion rates (e.g.  $D_A = 1 \times 10^{-10}$  cm<sup>2</sup> s<sup>-1</sup>, see figures 12 and 13) and 14).

The other purine, guanine, can be produced from AICA (L) (the hydrolysis product of AICN, reaction #12 of table 2), through a thermal reaction with either cyanogen (CN)<sub>2</sub> or cyanate. Cyanogen can be generated from HCN (H) either photochemically (107) or thermally (108); cyanate is obtained from cyanogen through hydrolysis (50). The production of guanine from AICA would increase the entropy production of the system, as can be seen by comparing the photon absorption characteristics of these two molecules, and would thus have been thermodynamically selected.

Regarding the pyrimidines; cytosine, uracil, and thymine, Ferris, Sanchez and Orgel (109) showed that on heating to 100 °C a 5:1 ratio of cyanate with cyanoacetylene, cytosine was formed in yields of 19%. In this reaction, cytosine

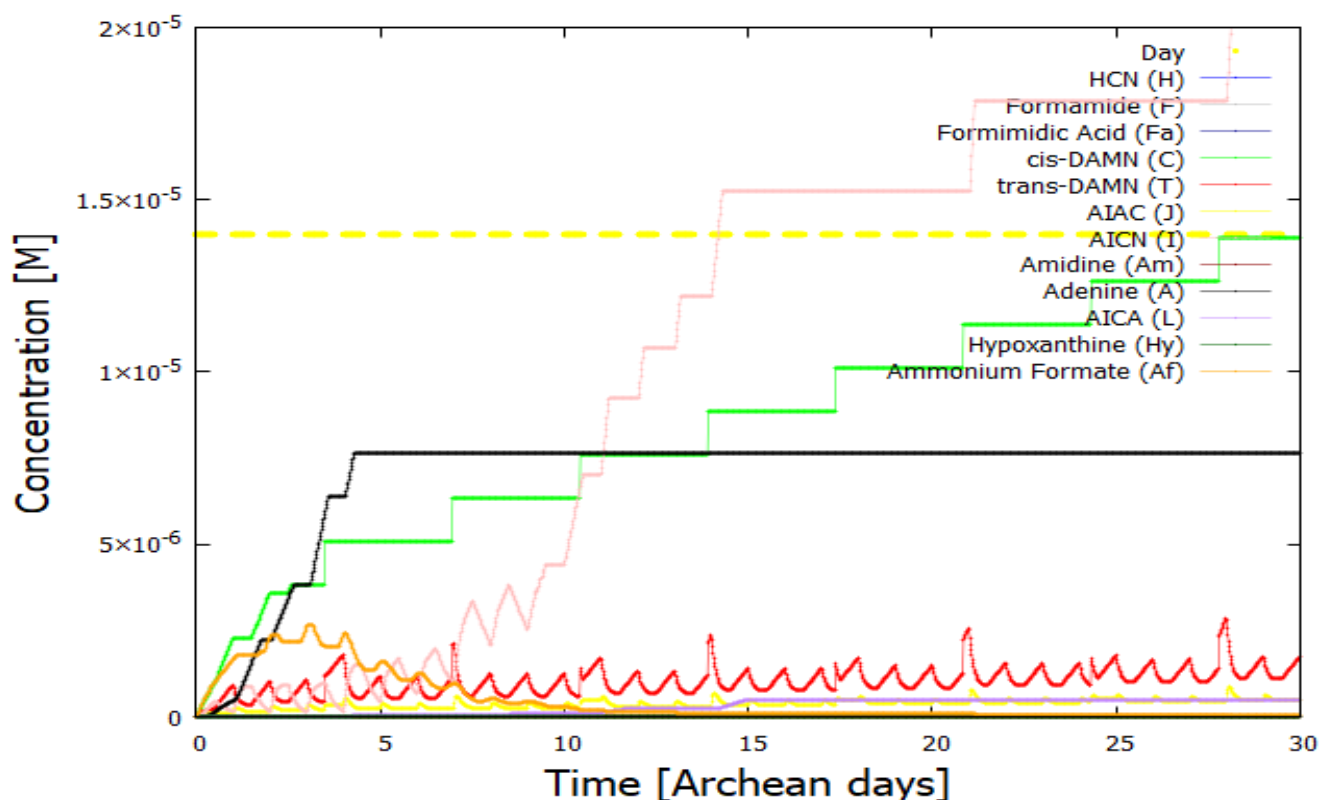


Figure 10: The same as Fig. 6, 80 °C, except with concentrations of HCN (H) and formimide at  $6 \times 10^{-4}$  and  $1 \times 10^{-4}$  M.

is formed mainly in a sequence involving the stable intermediate cyanovinylurea. Cyanogen or cyanofornamide can replace cyanate in this synthesis. Since cytosine hydrolyzes quite readily to uracil, and when uracil is reacted with formic acid in dilute aqueous solutions at 100–140 °C, thymine is formed (110), all of the pyrimidines can thereby be obtained. These photochemical and thermal reactions, leading to the dissipative structuring of the pyrimidines under the same wavelength region as the purines (adenine and guanine), also occurring within a fatty acid vesicle, will be considered in a future article.

## 7 Conclusions

I have presented the thermodynamics and photochemical reactions involved in the dissipative structuring, proliferation, and evolution of adenine as one of the fundamental molecules involved in the origin of life. More than the simple delineation of plausible routes to synthesis of particular molecules, and more than a fortuitous structuring of these which somehow fell under the providence of selection of chemical stability, and then natural selection, the origin of life presented here is considered as a spontaneous photochemical microscopic dissipative structuring process leading to strongly absorbing pigments with conical intersections which arise naturally to efficiently dissipate the impressed solar photon potential. The photochemical reactions required for the dissipative structuring necessarily occurred in the UVC region since this region has enough energy to directly break and reform double carbon covalent bonds while not enough energy to disassociate these molecules. Photochemical reactions are also much more diverse than thermal reactions and include tautomerizations, dissociations, radicalizations, isomerizations, charge transfers, additions, and substitutions, each providing a particular mechanism which could be employed in a given step of dissipative structuring.

For the organic precursor molecules like HCN and its hydrolysis product formamide, their conical intersections endow them with a significant non-adiabatic coupling of electronic degrees of freedom to nuclear vibrational degrees. At least for a short period of time, a local equilibrium of the molecules vibrational states is achieved after photon excitation and therefore Classical Irreversible Thermodynamic (CIT) theory can be applied to these photochemical

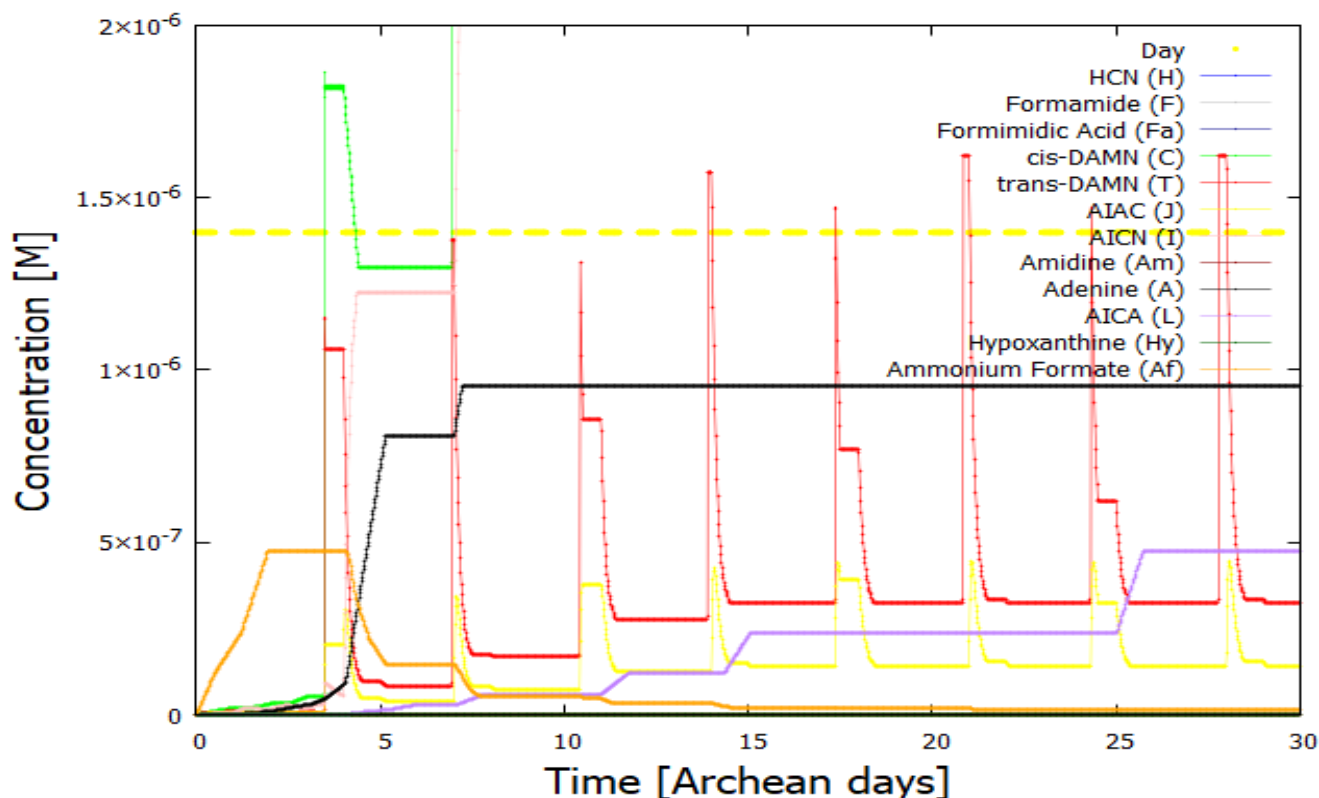


Figure 11: The same as Fig. 6, 80 °C, except with the diffusion exponential two orders of magnitude smaller,  $1.0 \times 10^{-8} \text{ cm}^2 \text{ s}^{-1}$  (e.g.  $D_A = 1.0 \times 10^{-8} \text{ cm}^2 \text{ s}^{-1}$ ).

reactions occurring in either the hot excited or hot ground states.

Evolution of the system is determined by two components; first, the likelihood of a microscopic fluctuation in the phase space of the internal molecular degrees of freedom which could potentially lead to a new molecular structure, and secondly, amplification in the non-linear regime (through autocatalysis) into new macroscopic flows of the incident energy (route of dissipation) corresponding to a new concentration profile of the products. The first component depends on the size of the “catchment basin” in the internal coordinate phase space (the shape of the conical intersection) that could lead to a new structure from the old structure. For example, if the new structure can be photochemically synthesized from the old structure over a wide range of absorbed photon energies then this structure would be more probable than others only obtainable from restricted photon wavelength regions. The second component is related to whether the new structure could act as a catalyst for its own production (non-linear regime). In this case, the new structure could be expected to increase its concentration, analogously to a catalyst in an autocatalytic thermal chemical reaction. Both these components foment the dissipation of the incident photon spectrum (foment entropy production) the first by presenting a broad absorption spectrum which happens to be the case for structures presenting one or more conical intersections leading to the required reaction pathway, and the second by increasing the flow of energy through the system due to an increase in the macroscopic amount (concentration) of such dissipative structures.

I have shown, using a simple vesicle model, how adenine can be synthesized and its concentration increased by more than 4 orders of magnitude over a relatively short period of 30 Archean days through periodic perturbations which lead the system to new stationary states of different product concentration with ever greater entropy production.

This molecular evolution process of dissipative structuring from common precursor molecules under UV light continues until reaching molecules with a broad absorption spectrum and which present a peaked conical intersection almost exclusively for internal conversion, thereby eliminating almost completely the possibility of further chemical reactions. Such molecules with peaked conical intersections and presenting broad absorption would then form a basis set of molecules for the dissipation of photons in yet more complex compound structures. It is neither a coincidence nor a requisite of stability that the fundamental molecules of life (those common to the three domains of

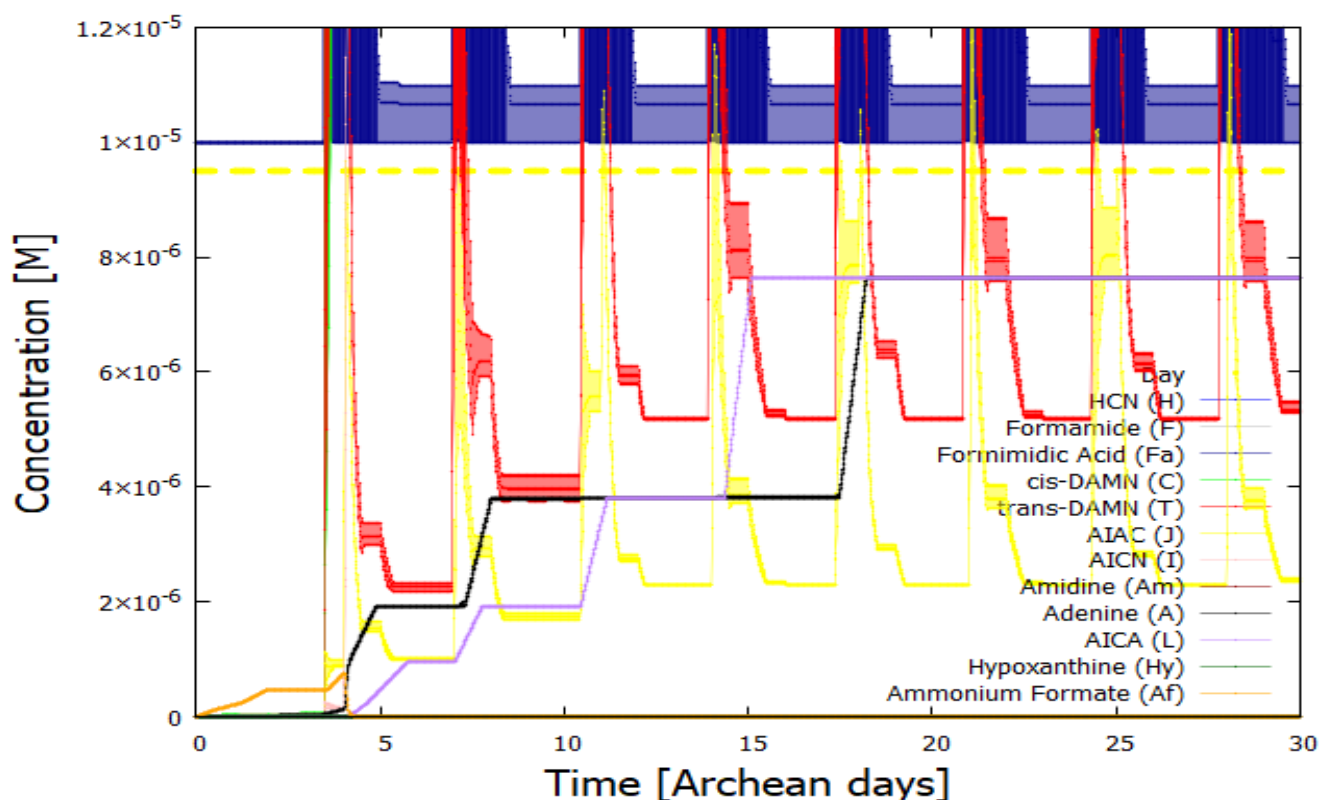


Figure 12: The same as Fig. 6, 80 °C, except with the diffusion exponential four orders of magnitude smaller,  $1.0 \times 10^{-10} \text{ cm}^2 \text{ s}^{-1}$  (e.g.  $D_A = 1.0 \times 10^{-10} \text{ cm}^2 \text{ s}^{-1}$ ). Six bins in depth  $x$  below the ocean surface are plotted until reaching the bottom of the 100  $\mu\text{m}$  (0.01 cm) vesicle. The top of the vesicle is at a depth of 0.00025 cm below the ocean surface. The small diffusion constant of  $1.0 \times 10^{-10} \text{ cm}^2 \text{ s}^{-1}$  allows the coupling of the reactions with diffusion leading to spatial symmetry breaking of the concentration profiles (see figures 13 and 14) and giving thicker lines because the 6 different depth bins are plotted.

life on Earth) have precisely these photochemical characteristics (figure 1) which are the “design” goals of dissipative structuring.

Dissipative structuring in biology has been ongoing, from the initial dissipation of the UVC + UVB wavelengths in the Archean by the dissipatively structured fundamental molecules of life, to the dissipation of wavelengths up to the red-edge by the organic pigments of today (7; 8; 12). From this perspective, evolution can be seen to have been overwhelmingly “concerned” with evolving complex biosynthetic pathways through this thermodynamic dissipative selection process to produce, proliferate, and support chromophores that could dissipate ever longer wavelengths, covering an ever greater region of the solar spectrum of higher intensity up to the red-edge. The simultaneous coupling of biotic with abiotic irreversible processes, such as ocean and air currents and the water cycle, allowed for dissipation towards still longer wavelengths beyond the red-edge (7; 111) culminating in an efficient global dissipating system known as the biosphere. Such a description of biotic-abiotic complexation leading to greater dissipation is described by classical irreversible thermodynamic theory in the non-linear regime. Irreversible processes and their coupling occur whenever physical and chemical constraints permit it and such coupling generally reduces impediments to greater global entropy production by introducing new microscopic degrees of freedom (112; 113; 114).

There is much empirical evidence for a thermodynamic selection towards states of increased dissipation in nature on vastly different size and time scales. For example, the increase in photon absorption and dissipation efficacy of a plant leaf over its lifetime (115), the fact that ecosystem succession correlates with increasing dissipation (116; 117), and the general increase in biosphere efficacy in photon dissipation (including the plant-induced increases in the water cycle (118; 119)) over evolutionary time. There is also evidence for this at the microscopic scale, for example in the increase in dissipation per unit biomass of the living cell over evolutionary history (120). Here I have shown that there exists evidence even at the nano-scale, for example, in the sequential increases in photon dissipation at each step during the microscopic dissipative synthesis of the molecule adenine under a UVC photon potential. This

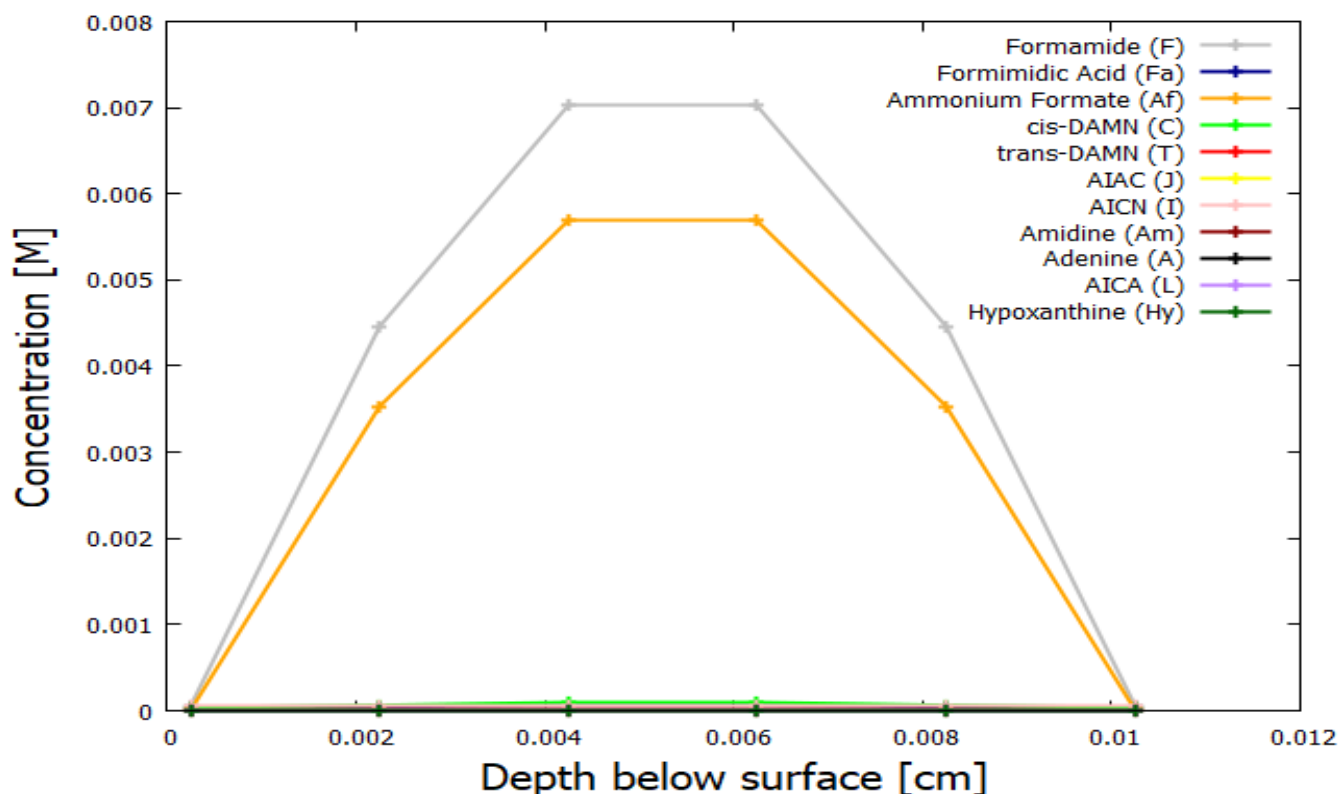


Figure 13: The concentration profile of the products as a function of depth below the ocean surface (the top of the vesicle is at a depth of 0.00025 cm below the surface) for the initial conditions of figure 12 and taken at the time of 7.3 Archean days. Six bins in depth  $x$  below the ocean surface are plotted until reaching the bottom of the 100  $\mu\text{m}$  (0.01 cm) vesicle.

is an example of dissipative selection at the molecular level. It is emphasized again that this is not akin to selection of chemical or photochemical stability because it is not related to maximizing entropy or minimizing the internal Gibb's free energy, but rather to increasing dissipation of the externally imposed photon potential, or, *increasing entropy production*.

It could then be expected that any planet around any star giving off light in the UVC region would have its own concentration profile of its own dissipatively synthesized carbon based fundamental molecules depending on the exact nature of the UV environment and the precursor and solvent molecules available locally. We have considered the synthesis of this basis set of molecules to be the first step of incipient life and this stage of life has therefore already been found on the other planets of our solar system, such as the UV sulfur containing pigments found in the clouds of Venus and the red chlorophyll-like pigments found on the surface of Mars and the UVC and UVB absorbing hydrocarbons found on Titan. For that matter, such molecular concentration profiles can, in fact, be found in interstellar gas clouds (12). Many of these interstellar fundamental molecules which are in a gas phase rather than a solvent environment turn out to be large polyaromatic hydrocarbons (12) and this could be understood from the fact that without the benefit of vibrational dissipation through hydrogen bonding to solvent water molecules, these space molecules in the gas phase need to be large in size in order to have many low frequency vibrational modes which would thereby increase dissipation. Dissipative structuring, dissipative proliferation, and dissipative selection are the necessary and sufficient elements to explain in physical-chemical terms the synthesis, proliferation, and complexation of organic molecules on planets and in interstellar space, and thus the origin and evolution of life on Earth.

In summary, the results presented here suggest the following conclusions;

1. The explanation for the origin of life cannot be equated with a list of scenarios for the synthesis of the fundamental organic molecules, but instead with a continuous dissipative process which allows for not only synthesis, but also proliferation and complexation seen in evolution, and this process, for carbon based life,

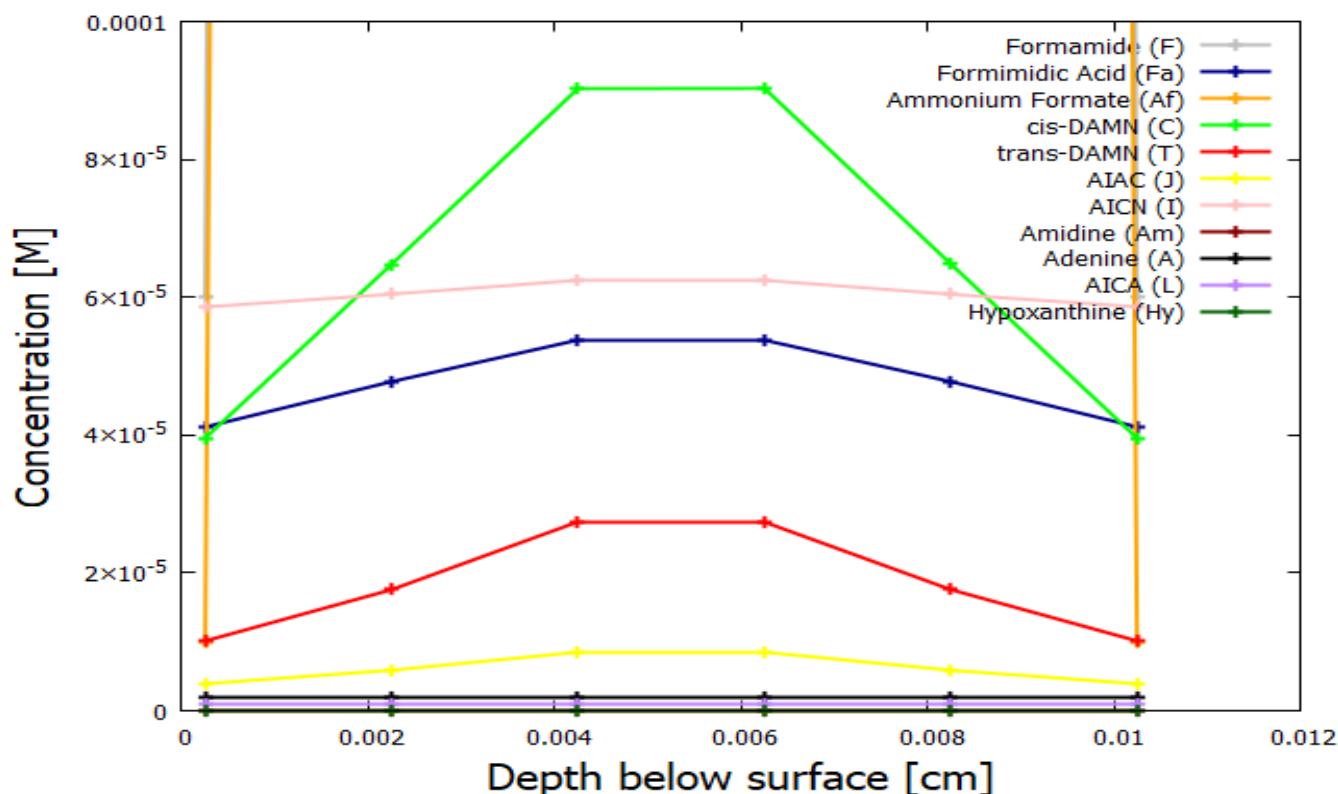


Figure 14: The same as figure 13 except with an expanded y-scale for the products of lesser concentration.

appears to have necessarily involved the dissipation of the UVC and UVB regions of the Archean solar spectrum.

2. A model in which the fundamental molecules are produced through photochemical and thermal reactions within a fatty acid vesicle permeable to HCN, H<sub>2</sub>O and formimidic acid (the photon-tautomerized hydrolysis product of HCN), but impermeable to the reaction products, allows for a significant build up of adenine and other reaction products, and would set the foundations for the beginning of cellular life.
3. High surface temperatures are necessary for copious production of adenine and this is in line with the geochemical fossil evidence of the Archean era.
4. Perturbations can lead the non-linear system into stationary states of greater product concentrations and it is reasonable to assume that these perturbations could have been caused by the vesicle floating into patches of higher concentration of HCN and formimidic acid existing at isolated regions of the ocean surface microlayer.
5. For very low diffusion rates, there appears to be a coupling of reactions with diffusion, leading to a non-homogeneous distribution of some of the intermediate products with a significantly greater concentration of these in the center of the vesicle. Such symmetry breaking could facilitate further structuring like polymerization.
6. The Glansdorff-Prigogine criterion indicating a decreasing contribution to the entropy production due to the variation of the forces (the affinities over the temperature), is obeyed in the photochemical and thermal structuring of the fundamental molecules. However, the *total* entropy production, including this structuring component due to variation of the affinities, plus a second contribution due to the variation of the flows of energy through the system, invariably increases over time. The system evolves towards final product molecules having an absorption maximum near the peak intensity of the incident UVC spectrum and with peaked conical intersections to internal conversion, both increasing the overall efficacy of dissipation of the incident solar spectrum.

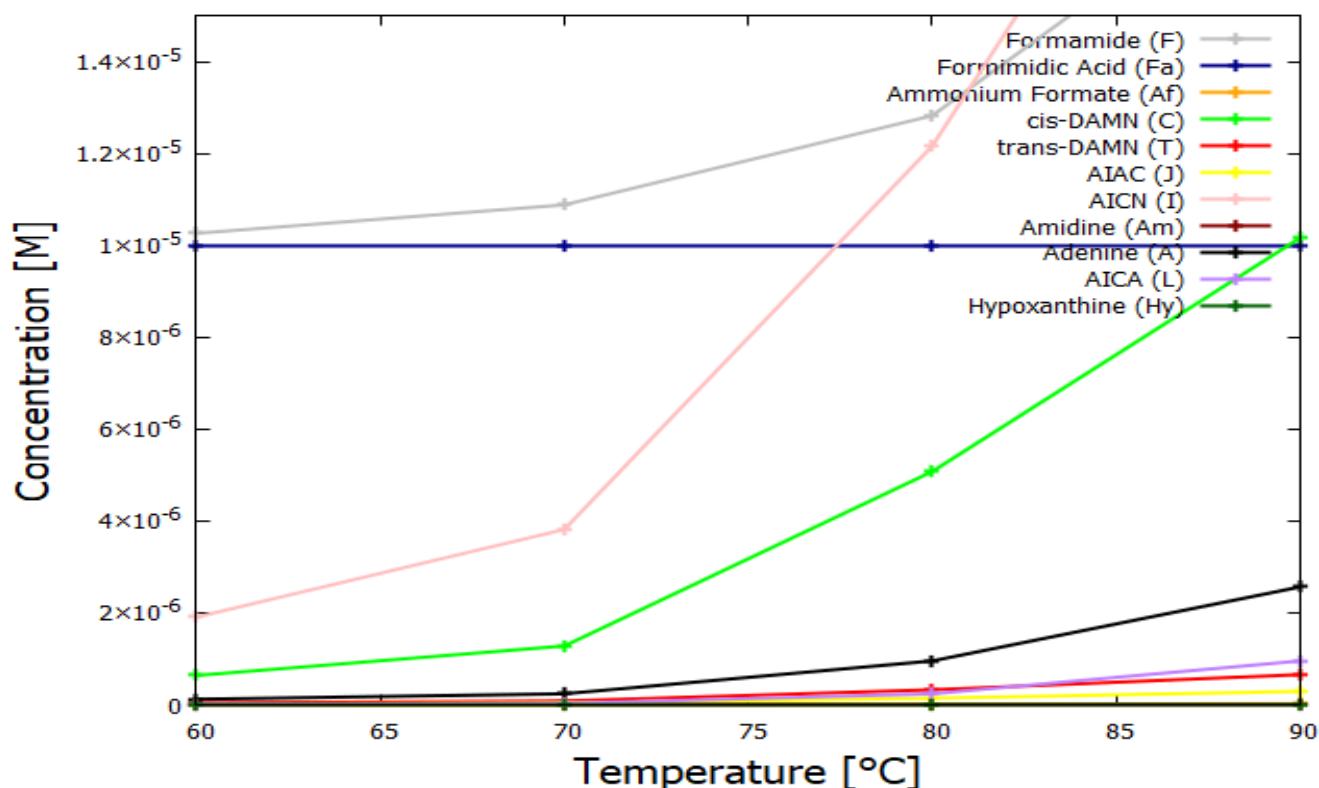


Figure 15: The temperature dependence of the concentrations of the product molecules, with the initial conditions,  $[H]=6E-05$ ,  $[F]=1E-05$ ,  $[Fa]=1E-05$  M, and all other molecules  $[ ]_0=1E-10$  and the diffusion constant  $D_A = 1.0 \times 10^{-6}$ , with perturbations.

- The dissipative structuring, proliferation, and evolution process has continued over the evolutionary history of life on Earth until today arriving at the red-edge ( $\sim 700$  nm) of the solar spectrum at Earth's surface. Beyond the red-edge, surface water absorbs strongly and dissipates photons efficiently. Furthermore, by fomenting the water cycle and ocean and wind currents, the irreversible process of life has evolved to couple with other irreversible processes, increasing further still the efficacy of solar photon dissipation into the far infrared.

## Appendix: Relation to Stability Theory

In the above I have applied the CIT formalism of Prigogine, Glansdorff and Nicolis to the photochemical dissipative structuring of adenine, one of the fundamental molecules of life, under a UVC photon potential at the ocean surface. Such an CIT analysis is sufficient to describe the synthesis, proliferation, and complexation of the fundamental molecules associated with the origin of life. In a non-linear system held under an imposed generalized thermodynamic force, multiple stationary states may exist. The system, upon perturbation may evolve from one stationary state to another. The only restriction on the direction of evolution is imposed by the universal evolutionary criterion of Glansdorff and Prigogine which indicates that the contribution to the entropy production due to changes during evolution of the free forces is always negative definite. There is, however, no restriction on the total entropy production which may either increase, decrease, or stay the same since there is another contribution to the entropy production due to the changes in the flows which has no definite sign. A complete stability analysis must be performed around the stationary state, normally, linear stability analysis does not suffice. However, for chemical or photochemical reactions, if there exist positive feedback, e.g. auto-catalysis or cross-catalysis, then the statistical tendency will generally be towards increasing overall dissipation of the applied chemical or photochemical potential and this has to do with the size of the catchment basins in the generalized phase space, which, in our case of microscopic dissipative structuring of molecules under UV light, are related to the conical intersections connecting the excited state to ground state for particular reaction coordinates. Only statistical probabilities for evolution can

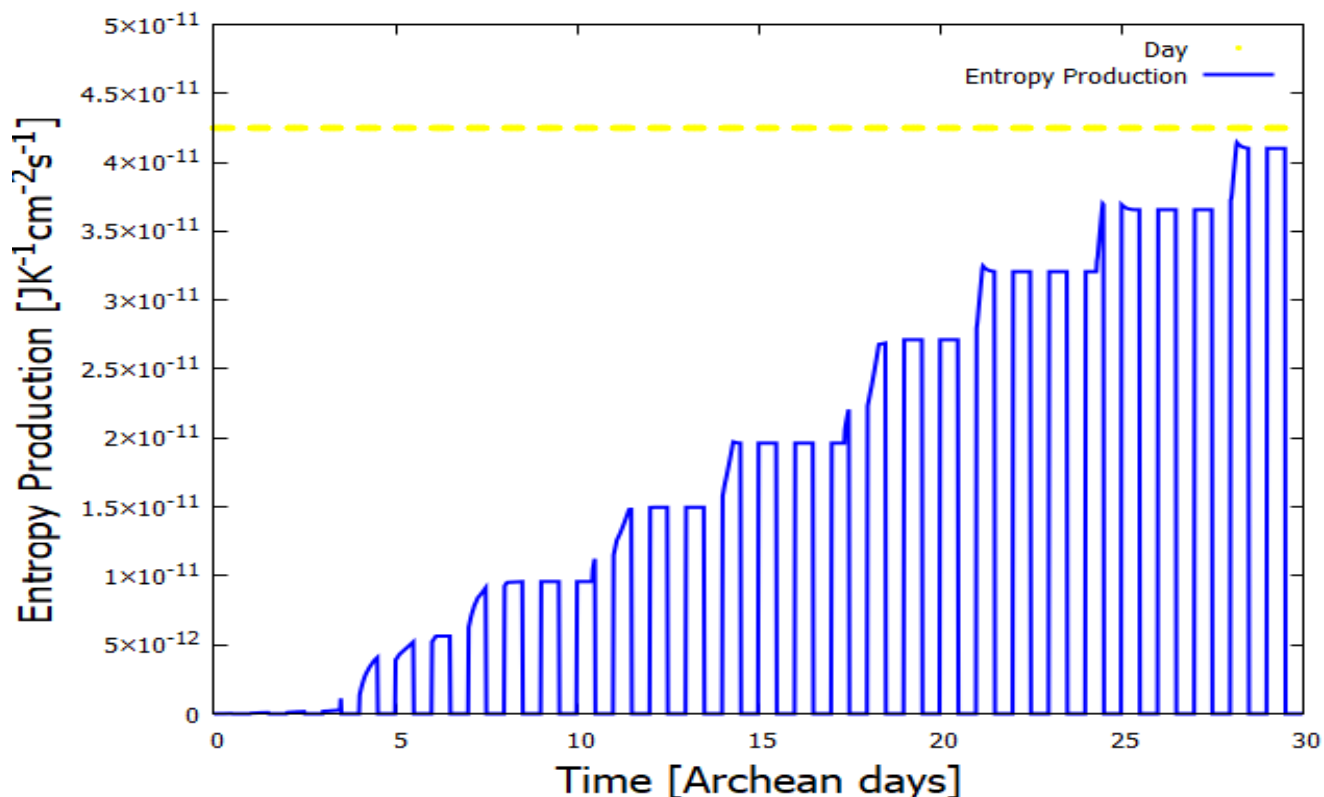


Figure 16: The production of entropy as a function of time during the photochemical dissipative structuring process leading to adenine at a sea surface temperature of 80 °C. The entropy production generally increases monotonically, but not always, and although it is the Glabdsdorf-Prigogine criterion, i.e. the reduction in entropy production due to the re-arrangement of the affinities, that drives the dissipative structuring of adenine, the total entropy production increases due to the increase in flow of energy from the incident source at a very hot temperature (the surface of the sun) to the emitted source of low temperature (the ocean surface temperature). At night, entropy production goes to zero. Although thermal chemical reactions still occur during the night, this entropy production is not included here.

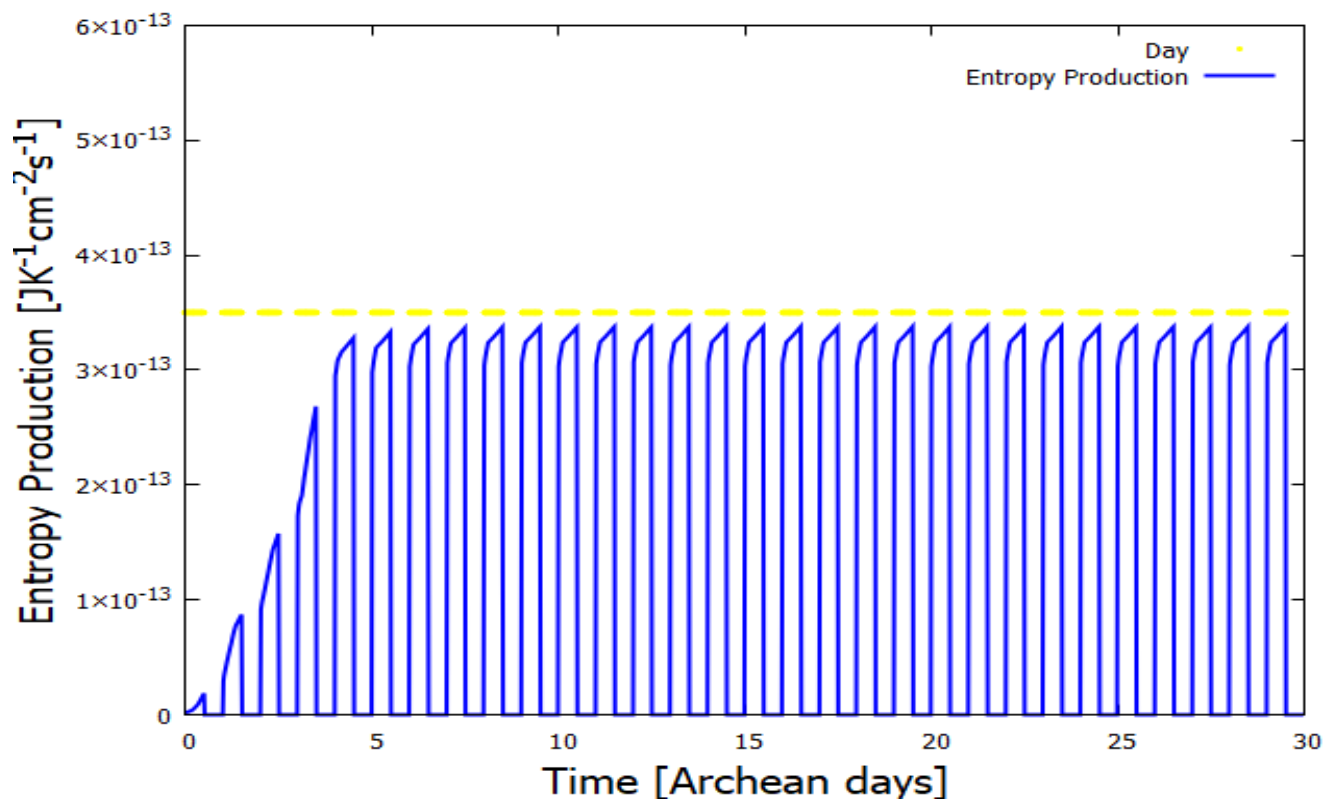


Figure 17: The production of entropy as a function of time during the photochemical dissipative structuring process leading to adenine at a sea surface temperature of  $80\text{ }^{\circ}\text{C}$ . Without perturbation of the vesicle, i.e. it does not pass through patches of increased HCN and Fa concentrations. The entropy production stabilizes at a value more than two orders of magnitude less than that of the perturbed system (figure 16).

be determined once these are delineated. Quantitatively, these will be specified by the quantum efficiencies for the particular photochemical reaction.

Since some recent works have considered general evolution of dissipative structures from a more restricted statistical mechanical framework using linear stability theory, here I establish the relationship between the more complete analysis given in section 2 using CIT theory and linear stability theory. In fact, Glansdorff and Prigogine did exactly this comparison for chemical reactions in their 1971 book (70) and what follows here is the photochemical analogue of their purely chemical analysis. It is emphasized that linear stability theory is a simplified and particular case of the CIT formalism corresponding to evolution only in the neighborhood of a stationary state and as such, contrary to what is occasionally claimed, it is not sufficient in itself to describe the evolution of a dissipative system.

The relation between the probability of a particular fluctuation occurring and entropy production was first considered by Einstein (121) who showed that for a Markovian and ergodic system under Gaussian fluctuations, the probability  $P$  of a fluctuation at the equilibrium state was related to the entropy change  $\Delta S$  by

$$P \propto \exp[\Delta S/k_B], \quad (22)$$

where  $k_B$  is the Boltzmann constant. Since at equilibrium entropy  $S$  is maximum,  $\Delta S$  due to a fluctuation must be negative, and thus the probabilities for fluctuations which lead the system away from equilibrium towards smaller entropy become exponentially smaller with the size of the decrease in entropy. Expanding the entropy to second order around the equilibrium state, for small fluctuations  $\Delta S$ , gives,

$$S = S_{eq} + (\delta S)_{eq} + \frac{1}{2}(\delta^2 S)_{eq} + \dots \quad (23)$$

For an isolated system at equilibrium  $S$  is a maximum, so  $(\delta S)_{eq} = 0$ , giving that  $\Delta S = S - S_{eq} \approx 1/2(\delta^2 S)_{eq}$ , and equation (22) can be rewritten

$$P \propto \exp[(\delta^2 S)_{eq}/2k_B]. \quad (24)$$

The quantity  $(\delta^2 S)_{eq}$  is known as the excess entropy (due to the fluctuation) and is always negative definite (since  $S_{eq}$  is a maximum). Since  $(\delta S)_{eq} = 0$  and  $(\delta^2 S)_{eq} < 0$ ,  $(\delta S)_{eq}$  is a Lyapunov function and the equilibrium state is stable.

This equilibrium Fluctuation Theorem was realized to also apply to non-equilibrium situations as long as the time scales associated with the fluctuating system are much shorter than the time scales associated with changes in the external boundary conditions. This was developed in detail by Onsager in 1931 (112; 113), and a few decades later by Callen and Welton (122), Onsager and Machlup (123), Kubo (124), Prigogine and Nicolis (125) and recently by Evans et al. (126) and Evans and Searles (127). In particular, Prigogine and Nicolis (125) made the theorem quantitative for non-equilibrium stationary states by extending Einstein's result to give (70),

$$P \propto \exp[(\delta^2 S)_0/2k_B] \quad (25)$$

where  $(\delta^2 S)_0$  is now calculated around a stationary non-equilibrium state. Using CIT theory it can be shown (70) that

$$\frac{\partial}{\partial t} \frac{1}{2}(\delta^2 S)_0 = \delta_X \sigma = \frac{1}{T} \sum_k \delta J_k \delta A_k, \quad (26)$$

where  $\delta_X \sigma$  is known as the excess entropy production (due to the current fluctuations  $\delta J_k$ ). In this non-equilibrium case,  $(\delta^2 S)_0$  plays the role of a Lyapunov function. The system will become unstable if processes become physically possible which give a negative contribution to the excess entropy production, and this can occur for autocatalytic and cross-catalytic reactions (70).

Starting with  $(\delta^2 S)_0 < 0$  around some stationary state, the system will always remain close and decay to this state which will correspond to the most probable configuration, as long as  $(\partial/\partial t)(\delta^2 S)_0$  is positive. However, for  $(\partial/\partial t)(\delta^2 S)_0$  negative,  $P$  will decrease. The system will then evolve to a new stationary state corresponding to a more probable state.

The work of Onsager, Prigogine, and Nicolis was recently generalized by Gaspard and Andrieux (128; 129; 130; 131) and given the name the "Stationary State Current-Fluctuation Theorem". According to this theorem, the probability  $P$  of observing a set of flows  $\mathbf{J}_\alpha$  at the stationary state with respect to that of observing their time reversed flows  $-\mathbf{J}_\alpha$  in the limit of large observational time  $t$  (i.e. in the time relaxed stationary state) is given by,

$$\frac{P(\mathbf{J}_\alpha)}{P(-\mathbf{J}_\alpha)} \approx \exp \left[ \frac{\mathbf{A}_\alpha \cdot \mathbf{J}_\alpha}{k_B T} \cdot V t \right] = \exp \left[ \frac{d_i S/dt}{k_B} \cdot t \right], \text{ for } t \rightarrow \infty, \quad (27)$$

where the last term is derived from equation (1), under the assumption of local equilibrium, and is just the exponential of the entropy production divided by the Boltzmann constant  $k_B$  times the time  $t$ . Therefore, given the possibility of two (or more) sets of flows  $\mathbf{J}_\alpha, \mathbf{J}_\beta, \dots$  corresponding to two (or more) sets of free affinities  $\mathbf{A}_\alpha, \mathbf{A}_\beta, \dots$  leading to two (or more) different values of the entropy production, in the non-linear regime where multiple stationary states are possible, current fluctuations which lead the system towards the state of greater dissipation are generally favored over time for amplification and this statistical rule for the selection of stationary states of dissipative systems we have termed *thermodynamic selection* (7; 8; 3) but we will use the term *dissipative selection* here in order to emphasize its origin, i.e. statistical selection of the configuration of greater dissipative efficacy. As with the Fluctuation Theorem, the Current-Fluctuation Theorem is not limited in its validity to macroscopic systems (the thermodynamic limit) nor is it limited to systems in local equilibrium. Local thermodynamic equilibrium is required only to validate the concept of entropy density in non-equilibrium situations and thus to associate dissipation with entropy production (the last term of Eq. (27)).

## Acknowledgments

The author is grateful to Carlos Bunge and Iván Santamaría-Holek for their revision of, and suggestions on, the manuscript and for the financial support of DGAPA-UNAM project number IN104920.

## References

- [1] I. Prigogine. *Introduction to Thermodynamics Of Irreversible Processes*. John Wiley & Sons, third edition, 1967.
- [2] L. Boltzmann. *Ludwig Boltzmann: Theoretical physics and philosophical problems: Selected writings*. 1974.
- [3] Karo Michaelian. *Thermodynamic Dissipation Theory of the Origina and Evolution of Life: Salient characteristics of RNA and DNA and other fundamental molecules suggest an origin of life driven by UV-C light*. Self-published. Printed by CreateSpace. Mexico City. ISBN:9781541317482., 2016.
- [4] S. L. Miller, H. C. Urey, and J. Oró. Origin of organic compounds on the primitive earth and in meteorites. *J. Mol. Evol.*, 9:59–72, 1976.
- [5] J. Oró, Miller S.L., and A. Lazcano. The origin and early evolution of life on earth. *Ann. Rev. Earth Planet. Sci.*, 18:317–356, 1990.
- [6] HJ Cleaves and SL Miller. Organic chemistry on the primitive earth and beyond. *Systems biology*, 1, 2007.
- [7] K. Michaelian. Thermodynamic origin of life. *ArXiv*, (<http://arxiv.org/abs/0907.0042>), 2009.
- [8] K. Michaelian. Thermodynamic dissipation theory for the origin of life. *Earth Syst. Dynam.*, 224:37–51, 2011.
- [9] L.V. Berkner and L.C. Marshall. *Origin and Evolution of the Oceans and Atmosphere*, pages 102–126. J. Wiley and Sons, 1964.
- [10] C. Sagan. Ultraviolet Selection Pressure on the Earliest Organisms. *J. Theor. Biol.*, 39:195–200, 1973.
- [11] I. Cnossen, J. Sanz-Forcada, O. Favata, F. and Witasse, T. Zegers, and N. F. Arnold. The habitat of early life: Solar x-ray and uv radiation at earth’s surface 4–3.5 billion years ago. *J. Geophys. Res.*, 112:E02008, 2007.
- [12] K. Michaelian and A. Simeonov. Fundamental molecules of life are pigments which arose and co-evolved as a response to the thermodynamic imperative of dissipating the prevailing solar spectrum. *Biogeosciences*, 12:4913–4937, 2015.
- [13] K. Michaelian. Microscopic dissipative structuring and proliferation at the origin of life. *Heliyon*, 3:e00424, 2017.
- [14] K. Michaelian and O. Rodriguez. Dissipative photochemical structuring of archean fatty acid vesicles. *Revista Cubana de Química*, 2019.
- [15] H. James Cleaves and Stanley L. Miller. Oceanic protection of prebiotic organic compounds from uv radiation. *Proceedings of the National Academy of Sciences*, 95(13):7260–7263, 1998.

- [16] Charles S. Cockell. The ultraviolet history of the terrestrial planets — implications for biological evolution. *Planetary and Space Science*, 48(2):203 – 214, 2000.
- [17] Armen Y. Mulkidjanian, Dmitry A. Cherepanov, and Michael Y. Galperin. Survival of the fittest before the beginning of life: selection of the first oligonucleotide-like polymers by uv light. *BMC Evolutionary Biology*, 3(1):12, May 2003.
- [18] A. I. Oparin. *Proiskhozhdenie zhizny (The origin of life)*. Weidenfeld and Nicholson, 1924.
- [19] Haldane J. B. S. Origin of life. *Rationalist Annual*, 148:3–10, 1929.
- [20] Harold C. Urey. On the early chemical history of the earth and the origin of life. *PNAS*, 38(4):351–363, 1952.
- [21] C. Sagan. Radiation and the origin of the gene. *Evolution*, 11:40–55, 1957.
- [22] Edward Charles Cyril Baly, W. E. Stephen, and N. R. Hood. The photosynthesis of naturally occurring compounds.&#x2014;ii. the photosynthesis of carbohydrates from carbonic acid by means of visible light. *Proceedings of the Royal Society of London. Series A, Containing Papers of a Mathematical and Physical Character*, 116(773):212–219, 1927.
- [23] Stanley L. Miller. A production of amino acids under possible primitive earth conditions. *Science*, 117(3046):528–529, 1953.
- [24] J. Oró and A.P. Kimball. Synthesis of purines under possible primitive earth conditions: Ii. purine intermediates from hydrogen cyanide. *Archives of Biochemistry and Biophysics*, 96(2):293 – 313, 1962.
- [25] C. Ponnampereuma, C. Sagan, and R. Mariner. Synthesis of adenosine triphosphate under possible primitive earth conditions. *Nature*, 199:222–226, 1963.
- [26] Ponnampereuma and R. Mariner. *Rad. Res.*, 19:183, 1963.
- [27] Ponnampereuma, R. Mariner, and C. Sagan. *Nature*, 198:1199, 1963.
- [28] J. P. Ferris and L. E. Orgel. An unusual photochemical rearrangement in the synthesis of adenine from hydrogen cyanide. *J. Am. Chem. Soc.*, 88:1074–1074, 1966.
- [29] Carl Sagan and Bishun N. Khare. Long-wavelength ultraviolet photoproduction of amino acids on the primitive earth. *Science*, 173(3995):417–420, 1971.
- [30] J. Mejía and K. Michaelian. Information encoding in nucleic acids through a dissipation-replication relation. *ArXiv*, 2018.
- [31] Michael Yarus, Joseph Widmann, and Rob Knight. RNA-Amino Acid Binding: A Stereochemical Era for the Genetic Code. *J Mol Evol*, 69(DOI 10.1007/s00239-009-9270-1):406–429, 2009.
- [32] K. Michaelian and A. Simeonov. Thermodynamic explanation of the cosmic ubiquity of organic pigments. *Astrobiol. Outreach*, 5:156, 2017.
- [33] Rayleigh. Some general theorems relating to vibrations. *Proc. Math. Soc. London*, 4:357–368, 1873.
- [34] A. Orr-Ewing. Reaction dynamics –relaxation pathways. *Lecture Notes*, pages 1–36, 2014.
- [35] Karl Kleinermanns, Dana Nachtigallová, and Mattanjah S. de Vries. Excited state dynamics of dna bases. *International Reviews in Physical Chemistry*, 32(2):308–342, 2013.
- [36] M. Barbatti, A.J. Aquino, J.J. Szymczak, D. Nachtigallová, P. Hobza, and H. Lischka. Relaxation mechanisms of uv-photoexcited dna and rna nucleobases. *Proc Natl Acad Sci U S A*, 107(50):21453–21458, 2010.
- [37] M. S. Schuurman and A. Stolow. Dynamics at conical intersections. *Annu. Rev. Phys. Chem.*, 69:427–450, 2018.
- [38] Polli et al. *Nature*, 467:440–443, 2010.

- [39] J. J. Serrano-Perez, F. de Vleeschouwer, F. de Proft, D. Mendive-Tapia, M. J. Bearpark, and M. A. Robb. How the conical intersection seam controls chemical selectivity in the photocycloaddition of ethylene and benzene. *J. Org. Chem.*, 78:1874–1886, 2013.
- [40] M. G. Trainer, J. L. Jimenez, Y. L. Yung, O. B. Toon, and M. A. Tolbert. Nitrogen incorporation in  $\text{CH}_4\text{-N}_2$  photochemical aerosol produced by far uv irradiation. *NASA archives*, 2012.
- [41] M. Ruiz-Bermejo, M. P. Zorzano, and S. Osuna-Esteban. Simple organics and biomonomers identified in hcn polymers: An overview. *Life*, 3:421–448, 2013.
- [42] D. Ritson and J. Sutherland. Prebiotic synthesis of simple sugars by photoredox systems chemistry. *Nature Chem.*, 4:895–899, 2012.
- [43] Tamal Das, Siddharth Ghule, and Kumar Vanka. Insights into the origin of life: Did it begin from hcn and  $\text{H}_2\text{O}$ ? *ACS Central Science*, 5(9):1532–1540, 2019.
- [44] E. Pflüger. Beiträge zur lehre von der respiration. i. ueber die physiologische verbrennung in den lebendigen organismen. *Arch. Ges. Physiol.*, 10:641–644, 1875.
- [45] R. D. Minard and C. N. Matthews. Hcn world: Establishing proteinucleic acid life via hydrogen cyanide polymers. *Abstr. Pap. Am. Chem. Soc.*, 228:U963–U963, 2004.
- [46] C. N. Matthews. *Series: Cellular Origin and Life in Extreme Habitats and Astrobiology*, volume 6, chapter The HCN World, pages 121–135. Kluwer, Dordrecht, 2004.
- [47] Marc Neveu, Hyo-Joong Kim, and Steven A. Benner. The “strong” rna world hypothesis: Fifty years old. *Astrobiology*, 13(4):391–403, 2013. PMID: 23551238.
- [48] E. Boulanger, A. Anoop, D. Nachtigallova, W. Thiel, and M. Barbatti. Photochemical steps in the prebiotic synthesis of purine precursors from hcn. *Angew. Chem. Int.*, 52:8000–8003, 2013.
- [49] J. Oró. *Biochem. Biophys. Res. Commun.*, 2:407–412, 1960.
- [50] R. A. Sanchez, J. P. Ferris, and L. E. Orgel. Studies in prebiotic synthesis ii: Synthesis of purine precursors and amino acids from aqueous hydrogen cyanide. *J. Mol. Biol.*, 80:223–253, 1967.
- [51] R. A. Sanchez, J. P. Ferris, and L. E. Orgel. Studies in prebiotic synthesis iv: Conversion of 4-aminoimidazole-5-carbonitrile derivatives to purines. *J. Mol. Biol.*, 38:121–128, 1968.
- [52] D. Roy, K. Najafian, and P. von Rague Schleyer. Chemical evolution: The mechanism of the formation of adenine under prebiotic conditions. *PNAS*, 104(44):17272–17277, October 2007.
- [53] R. Stribling and S. L. Miller. Energy yields for hydrogen cyanide and formaldehyde syntheses: The hcn and amino acid concentrations in the primitive ocean. *Origins Life*, 17:261–273, 1986.
- [54] R. Sanchez, J. Ferris, and L. E. Orgel. Conditions for purine synthesis: Did prebiotic synthesis occur at low temperatures? *Science*, 153(3731):72–73, 1966.
- [55] S. L. Miller and A. Lazcano. The origin of life – did it occur at high temperatures? *Mol. Evol.*, 41:689–692, 1995.
- [56] Jeffrey L. Bada and Antonio Lazcano. Some like it hot, but not the first biomolecules. *Science*, 296:1982–1983, 2002.
- [57] S. Miyakawa, H. J. Cleaves, and S. L. Miller. The cold origin of life: B. implications based on pyrimidines and purines produced from frozen ammonium cyanide solutions. *Origins of Life and Evolution of the Biosphere*, 32:209–218, 2002.
- [58] J. T. Hardy. The sea-surface microlayer (1982) biology, chemistry and anthropogenic enrichment. *Prog. Oceanogr.*, 11:307–328, 1982.
- [59] M. Grammatika and W. B. Zimmerman. Microhydrodynamics of flotation processes in the sea-surface layer. *Dynam. Atmos. Oceans*, 34:327–348, 2001.

- [60] Balázs Fábrián, Milán Szóri, and Pál Jedlovsky. Floating patches of hcn at the surface of their aqueous solutions – can they make “hcn world” plausible? *The Journal of Physical Chemistry C*, 118(37):21469–21482, 2014.
- [61] Ye Fan, Yun Fang, and Lin Ma. The self-crosslinked ufasome of conjugated linoleic acid: Investigation of morphology, bilayer membrane and stability. *Colloids and Surfaces B: Biointerfaces*, 123:8 – 14, 2014.
- [62] Jerry Han and Melvin Calvin. Occurrence of fatty acids and aliphatic hydrocarbons in a 3.4 billion-year-old sediment. *Nature*, 224(5219):576–577, 1969.
- [63] William Van Hoesen, JR Maxwell, and Melven Calvin. Fatty acids and hydrocarbons as evidence of life processes in ancient sediments and crude oils. *Geochimica et Cosmochimica Acta*, 33(7):877–881, 1969.
- [64] J. Karhu and S. Epstein. The implication of the oxygen isotope records in coexisting cherts and phosphates. *Geochim. Cosmochim. Acta*, 50:1745–1756, 1986.
- [65] L. P. Knauth. *Lecture Notes in Earth Sciences #43*, chapter Isotopic Signatures and Sedimentary Records, pages 123–152. Springer-Verlag, Berlin, 1992.
- [66] L. P. Knauth and D. R. Lowe. High archaic climatic temperature inferred from oxygen isotope geochemistry of cherts in the 3.5 ga swaziland group, south africa. *Geol. Soc. Am. Bull.*, 115:566–580, 2003.
- [67] A. M. Schoffstall. Prebiotic phosphorylation of nucleosides in formamide. *Origins Life Evol Biosphere*, 7:399–412, 1976.
- [68] G. Costanzo, R. Saladino, C. Crestini, F. Ciciriello, and E. Di Mauro. Nucleoside phosphorylation by phosphate minerals. *J Biol Chem.*, 282(23):16729–16735, 2007.
- [69] A. M. Turing. The Chemical Basis of Morphogenesis. *Philosophical Transactions of the Royal Society of London Series B*, 237(641):37–72, August 1952.
- [70] P. Glansdorff and I. Prigogine. *Thermodynamic Theory of Structure, Stability and Fluctuations*. Wiley - Interscience., 1971.
- [71] Christian Petersen, Niels Henning Dahl, Svend Knak Jensen, Jens Aage Poulsen, Jan Thøgersen, and Søren Rud Keiding. Femtosecond photolysis of aqueous formamide. *The Journal of Physical Chemistry A*, 112(15):3339–3344, 2008. PMID: 18321081.
- [72] Harold Basch, M. B. Robin, and N. A. Kuebler. Electronic spectra of isoelectronic amides, acids, and acyl fluorides. *The Journal of Chemical Physics*, 49(11):5007–5018, 1968.
- [73] F. Lelj and C. Adamo. Solvent effects on isomerization equilibria: An energetic analysis in the framework of density functional theory. *Theoretica chimica acta*, 91:199–214, 1995.
- [74] T.H. Koch and R.M. Rodehorst. Quantitative investigation of the photochemical conversion of diaminomaleonitrile to diaminofumaronitrile and 4-amino-5-cyanoimidazole. *J. Am. Chem. Soc.*, 96:6707–6710, 1974.
- [75] V.P. Gupta and Poonam Tandon. Conformational and vibrational studies of isomeric hydrogen cyanide tetramers by quantum chemical methods. *Spectrochimica Acta Part A: Molecular and Biomolecular Spectroscopy*, 89:55 – 66, 2012.
- [76] JP Ferris, PC Joshi, EH Edelson, and JG Lawless. Hcn: a plausible source of purines, pyrimidines and amino acids on the primitive earth. *Journal of molecular evolution*, 11(4):293–311, 1978.
- [77] R. Glaser, B. Hodgen, D. Farrelly, and E. McKee. Adenine synthesis in interstellar space: mechanisms of prebiotic pyrimidine-ring formation of monocyclic hcn-pentamers. *Astrobiology*, 7(3):455–470, 2007.
- [78] M. J. Cavaluzzi and P. N. Borer. Revised uv extinction coefficients for nucleoside-5'- monophosphates and unpaired dna and rna. *Nucleic Acids Research*, 32(1):e13, 2004.
- [79] J. Franz and F.A. Gianturco. Low-energy positron scattering from dna nucleobases: the effects from permanent dipoles. *Eur. Phys. J. D*, 68:279–??, 2014.

- [80] Miriam Michael Stimson and Mary Agnita Reuter. Ultraviolet absorption spectra of nitrogenous heterocycles. vii. the effect of hydroxy substitutions on the ultraviolet absorption of the series: Hypoxanthine, xanthine and uric acid1. *Journal of the American Chemical Society*, 65(2):153–155, 1943.
- [81] S. Miyakawa, H. J. Cleaves, and S. L. Miller. The cold origin of life: A. implications based on the hydrolytic stabilities of hydrogen cyanide and formamide. *Origins of Life and Evolution of the Biosphere*, 32:195–208, 2002.
- [82] Jeremy Kua and Kyra L. Thrush. Hcn, formamidic acid, and formamide in aqueous solution: A free-energy map. *The Journal of Physical Chemistry B*, 120(33):8175–8185, 2016. PMID: 27016454.
- [83] Günther Maier and Jörg Endres. Isomerization of matrix-isolated formamide: Ir-spectroscopic detection of formimidic acid. *European Journal of Organic Chemistry*, 2000(6):1061–1063, 2000.
- [84] F. Duvernay, A. Trivella, F. Borget, S. Coussan, J. P. Aycard, and T. Chiavassa. Matrix isolation fourier transform infrared study of photodecomposition of formimidic acid. *J. Phys. Chem. A*, 109:11155–11162, 2005.
- [85] et al. Barks, H.L. Guanine, adenine, and hypoxanthine production in uv-irradiated formamide solutions: relaxation of the requirements for prebiotic purine nucleobase formation. *Chembiochem*, 11:1240–1243, 2010.
- [86] J.M. Gingell, N.J. Mason, H. Zhao, I.C. Walker, and M.R.F. Siggel. Vuv optical-absorption and electron-energy-loss spectroscopy of formamide. *Chemical Physics*, 220(1):191 – 205, 1997.
- [87] E. Yonemitsu, T. Isshiki, and Y. Kijima. Process for preparing adenine, 1974. US Patent 4,059,582.
- [88] G. Zubay and T. Mui. Prebiotic synthesis of nucleotides. *Orig Life Evol Biosph*, 31:87–102, 2001.
- [89] Jing Wang, Jiande Gu, Minh Tho Nguyen, Greg Springsteen, and Jerzy Leszczynski. From formamide to purine: A self-catalyzed reaction pathway provides a feasible mechanism for the entire process. *The Journal of Physical Chemistry B*, 117(32):9333–9342, 2013. PMID: 23902343.
- [90] M. Levy and S. L. Miller. The stability of the rna bases: Implications for the origin of life. *Proc. Natl. Acad. Sci. USA*, 95:7933–7938, 1998.
- [91] Shiliang Wang and Anguang Hu. Comparative study of spontaneous deamination of adenine and cytosine in unbuffered aqueous solution at room temperature. *Chemical Physics Letters*, 653:207 – 211, 2016.
- [92] Xiao Chuan Wang, Jeff Nichols, Martin Feyereisen, Maciej Gutowski, Jerry Boatz, A. D. J. Haymet, and Jack Simons. Ab initio quantum chemistry study of formamide-formamidic acid tautomerization. *The Journal of Physical Chemistry*, 95(25):10419–10424, 1991.
- [93] Franco Cataldo, Giacomo Patanè, and Giuseppe Compagnini. Synthesis of hcn polymer from thermal decomposition of formamide. *Journal of Macromolecular Science, Part A*, 46(11):1039–1048, 2009.
- [94] A. Hill and L.E. Orgel. Synthesis of adenine from hcn tetramer and ammonium formate. *Orig Life Evol Biosph*, 32:99–102, 2002.
- [95] Eric Herbst. The chemistry of interstellar space. *Chem. Soc. Rev.*, 30:168–176, 2001.
- [96] Abdelilah Benallou. A new mechanistic insight of dna base adenine formation from pentamer hcn in the gas phase of interstellar clouds. *Journal of Taibah University for Science*, 13(1):105–111, 2019.
- [97] Rafał Szabla, Judit E. Šponer, Jiří Šponer, Andrzej L. Sobolewski, and Robert W. Góra. Solvent effects on the photochemistry of 4-aminoimidazole-5-carbonitrile, a prebiotically plausible precursor of purines. *Phys. Chem. Chem. Phys.*, 16:17617–17626, 2014.
- [98] G. Frick. Formation of amino-acids in hydrolysis of adenine. *Nature*, 169:758–759, 1952.
- [99] H. Zheng and F. Meng. Theoretical study of water-assisted hydrolytic deamination mechanism of adenine. *Struct Chem*, 20:943–949, 2009.

- [100] A. Luna, J.-P. Morizur, J. Tortajada, M. Alcamí, O. Mó, and M. Yáñez. Role of  $\text{Cu}^+$  association on the formamide  $\rightarrow$  formamidylic acid  $\rightarrow$  (aminohydroxy)carbene isomerizations in the gas phase. *The Journal of Physical Chemistry A*, 102(24):4652–4659, 1998.
- [101] N. J. Yang and M. J. Hinner. Getting across the cell membrane: An overview for small molecules, peptides, and proteins. *Methods Mol Biol.*, 1266:29–53, 2015.
- [102] S. Agarwal, C. Clancy, and R. Harvey. Mechanisms restricting diffusion of intracellular  $\text{Ca}^{2+}$ . *Sci. Rep.*, 6:19577, 2008.
- [103] William J. Bowen and Harold L. Martin. The diffusion of adenosine triphosphate through aqueous solutions. *Archives of Biochemistry and Biophysics*, 107(1):30 – 36, 1964.
- [104] Kevin J. Zahnle. Photochemistry of methane and the formation of hydrocyanic acid (hcn) in the earth’s early atmosphere. *Journal of Geophysical Research: Atmospheres*, 91(D2):2819–2834, 1986.
- [105] C. Chyba and C. Sagan. Endogenous production, exogenous delivery and impact-shock synthesis of organic molecules: an inventory for the origins of life. *Nature*, 355:125–132, 1992.
- [106] ZHANG Z., C. LIU, L. LIU, L. YU, and Z. WANG. Study on dissolved trace metals in sea surface microlayer in daya bay. *Chinese Journal of Oceanology and Limnology*, 22(1):54 – 63, 2004.
- [107] P. L. Airey and Frederick Sydney Dainton. The photochemistry of aqueous solutions of  $\text{Fe}(\text{II})$ . Processes in acidified solutions of potassium ferrocyanide at 25°C. *Proceedings of the Royal Society of London. Series A. Mathematical and Physical Sciences*, 291(1427):478–486, 1966.
- [108] Sidney W. Fox and Kaoru Harada. Synthesis of uracil under conditions of a thermal model of prebiological chemistry. *Science*, 133(3468):1923–1924, 1961.
- [109] J. P. Ferris, R. A. Sanchez, and L. E. Orgel. Studies in prebiotic synthesis iii. synthesis of pyrimidines from cyanoacetylene and cyanate. *J. Mol. Biol.*, 33:693–704, 1968.
- [110] A.S.U. Choughuley, A.S. Subbaraman, Z.A. Kazi, and M.S. Chadha. A possible prebiotic synthesis of thymine: Uracil-formaldehyde-formic acid reaction. *Biosystems*, 9(2):73 – 80, 1977. Fifth international conference on the origin of life.
- [111] K. Michaelian. Biological catalysis of the hydrological cycle: life’s thermodynamic function. *Hydrol. Earth Syst. Sci.*, 16:2629–2645, 2012.
- [112] L. Onsager. Reciprocal Relations in Irreversible Processes, I. *Phys. Rev.*, 37:405–426, 1931.
- [113] L. Onsager. Reciprocal Relations in Irreversible Processes, II. *Phys. Rev.*, 38:2265, 1931.
- [114] R. E. Morel and G. Fleck. Onsager’s principle: A unifying biotheme. *J. Theor. Biol.*, 136:171–175, 1989.
- [115] D. M. Gates. *Biophysical Ecology*. Springer-Verlag, 1980.
- [116] R.E. Ulanowicz and B.M. Hannon. Life and the production of entropy. *Proc R Soc Lond B*, 232:181–192, 1987.
- [117] E. D. Schneider and J. J. Kay. Complexity and thermodynamics: towards a new ecology. *Futures*, 24:626–647, 1994.
- [118] Axel Kleidon. Entropy production by evapotranspiration and its geographic variation. *Soil & Water Res.*, 3:S89–S94, 2008.
- [119] K. Michaelian. *The Biosphere*, chapter The biosphere: A thermodynamic imperative. INTECH, 2012.
- [120] A. I. Zotin. *Bioenergetic trends of evolutionary progress of organisms*, pages 451–458. De Gruyter, 1984.
- [121] A. Einstein. *Ann. Phys.*, (17):549, 1905.
- [122] H. B. Callen and T. A. Wellton. Irreversibility and generalized noise. *Physical Review*, 83:34–40, 1951.
- [123] L. Onsager and S. Machlup. Fluctuations and irreversible processes. *Phys. Rev.*, 91:1505–1512, 1953.

- [124] R. Kubo. The fluctuation-dissipation theorem. pages 255–284, 1966.
- [125] I. Prigogine and G. Nicolis. Biological order, structure and instabilities. *Quarterly Reviews of Biophysics*, 4:107–144, 1971.
- [126] D. J. Evans, E. G. D. Cohen, and G. P. Morriss. Probability of second law violations in shearing steady states. *Physical Review Letters*, 71(15):2401–2404, 1993.
- [127] D. J. Evans, E. G. D. Cohen, and G. P. Morriss. The fluctuation theorem. *Advances in Physics*, 51(7):1529–1585, 2002.
- [128] P. Gaspard. *Engineering of Chemical Complexity*, chapter Self-Organization at the Nanoscale Scale in Far-From-Equilibrium Surface Reactions and Copolymerizations, pages 51–77. World Scientific, 2013.
- [129] Pierre Gaspard. Fluctuation theorem for nonequilibrium reactions. *The Journal of Chemical Physics*, 120(19):8898–8905, 2004.
- [130] D. Andrieux and P. Gaspard. Fluctuation theorem for currents and schnakenberg network theory. *J. Stat. Phys.*, 127:107–131, 2007.
- [131] D Andrieux, P Gaspard, T Monnai, and S Tasaki. The fluctuation theorem for currents in open quantum systems. *New Journal of Physics*, 11(4):043014, apr 2009.